Thermoresponsive Cell Culture Substrates Based on PNIPAM Brushes Functionalized with Adhesion Peptides: Theoretical Considerations of Mechanism and Design

ARTICLE *in* LANGMUIR · NOVEMBER 2012

Impact Factor: 4.46 · DOI: 10.1021/la303443t · Source: PubMed

2 AUTHORS:

Avraham Halperin
French National Centre for Scientific Research
119 PUBLICATIONS **3,918** CITATIONS
SEE PROFILE

Martin Kröger
ETH Zurich
239 PUBLICATIONS **3,842** CITATIONS
SEE PROFILE

Langmuir

Article

pubs.acs.org/Langmuir

Thermoresponsive Cell Culture Substrates Based on PNIPAM Brushes Functionalized with Adhesion Peptides: Theoretical Considerations of Mechanism and Design

Avraham Halperin*,† and Martin Kröger*,‡

†University of Grenoble 1/CNRS, LIPhy UMR 5588, BP 87, 38041 Grenoble, France

‡Polymer Physics, Department of Materials, ETH Zurich, CH-8093 Zurich, Switzerland

ABSTRACT: Thermoresponsive tissue culture substrates based on PNIPAM brushes are used to harvest confluent cell sheets for tissue engineering. The prospect of clinical use imposes the utilization of culture medium free of bovine serum, thus suggesting conjugation with adhesion peptides containing the RGD minimal recognition sequence. The optimum position of the RGD along the chain should ensure both cell adhesion at 37 °C and cell detachment at T_L below the lower critical solution temperature of PNIPAM. Design guidelines are formulated from considerations of brush confinement by the cells: (i) Cell adhesion at 37 °C is controlled by the RGDs accessible without brush compression. (ii) Cell detachment at T_L is driven by a disjoining force due to confinement of the swollen brush by cells retaining integrin−RGD bonds formed at 37 °C. These suggest placing the RGDs at the grafting surface or its vicinity. Randomly placed RGDs do not enable efficient detachment because a large fraction of the integrin−RGD bonds are not sufficiently tensioned at T_L, in line with experimental observations (Ebara, M.; Yamato, M.; Aoyagi, T.; Kikuchi, A.; Sakai, K.; Okano, T. Immobilization of celladhesive peptides to temperature-responsive surfaces facilitates both serum-free cell adhesion and noninvasive cell harvest. *Tissue Eng.* **2004**, *10*, 1125−1135). The theory framework enables analysis of culture media based on polymer brushes conjugated with adhesion peptides in general.

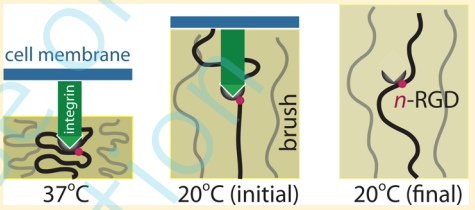

1. INTRODUCTION

Temperature responsive tissue culture substrates enable the harvesting of confluent cell sheets with intact cell−cell junctions and extracellular matrix (ECM).[1−6] This is of interest because of the potential for regenerative medicine applications known as cell sheet engineering. The thermoresponsive substrates consist of surface layers of poly(*N*-isopropylacrylamide) (PNIPAM) of various architectures including electron beam (e-b) cross-linked hydrogels,[4,5,7] adsorbed PNIPAM chains,[8] brushes,[9−15] plasma polymerized layers,[16−20] and microgels.[21] They allow cell adhesion and proliferation at 37 °C, above the bulk lower critical transition temperature (LCST) of PNIPAM at $T_{LCST} \approx 26$ °C. The cells spontaneously detach upon lowering the temperature to T_L below the LCST, and efficient harvesting is typically achieved at $T_L = 20$ °C. Brush based substrates are of special interest because their physical properties and interactions with cells can be controlled by tuning two parameters, the area per chain, Σ, and the polymerization degree, N. This in turn suggests the possibility of rational design to optimize the performance of the substrate to specifically accommodate different cell types.[12] However, the prospect of eventual clinical applications introduces additional design considerations aiming to eliminate xenogenic components from the cell culture process.[22] This issue arises because cell adhesion to PNIPAM brush substrates is typically promoted by use of serum-containing growth medium. The physical adsorption of the serum borne extracellular matrix (ECM) proteins fibronectin (FN) and vitronectin (VN) provides ligands to integrin receptors anchored to the cell membrane, thus enhancing cell adhesion and proliferation.[23] In turn, the formulation of the serum based culture medium typically involves fetal bovine serum (FBS), thus raising concerns of contamination by animal disease and immune-reaction to foreign proteins.[22] An approach resolving this problem involves functionalization PNIPAM with pendant adhesive peptides such as RGDs (Arg-Gly-Asp-Ser).[24−27] It was explored for e-b hydrogels and was demonstrated to allow cell culture in serum free medium. The implementation of this strategy to PNIPAM brushes remains to be explored experimentally.

In the following, we present theoretical considerations concerning the design of such functionalized brushes to enable cell adhesion at 37 °C and efficient detachment at $T_L < T_{LCST}$. For specificity, we consider short adhesion peptides containing the RGD minimal recognition sequence and attached to the nth monomers along the chains, $1 \le n \le N$. In the following, we refer to such RGD bearing monomers as n-RGDs. Our analysis aims to characterize the effect of n/N on both cell adhesion and detachment. Enhancing the two processes individually poses different requirements, and we identify an optimal n/N range and its dependence on Σ. Based on the n-RGD results, we consider also the case of RGD randomly positioned along the chain, ran-RGD, as specified by the fraction of functionalized monomers. In this case, our analysis suggests slower detach-

Received: August 27, 2012
Revised: November 2, 2012
Published: November 2, 2012

ment, thus affording a possible rationalization of the experimental results of Ebara et al.[24,25] The interest in the theoretical analysis of this system is threefold: First, design guidelines for such systems are of practical interest for "brush based" cell sheet engineering. Second, the analysis suggests experimental probes of the mechanism of function of PNIPAM brush substrates. Finally, from polymer theory point of view, our discussion extends early results[28,29] on the spatial distribution of the nth monomer within the brush. In addition, it introduces analytical approximations for the description of PNIPAM brushes.

For concreteness, our discussion focuses on substrates comprising PNIPAM brushes and RGD adhesion peptides. Their modeling draws on extensive studies of their physical chemistry and cell culture characteristics. However, the theoretical framework can be applied to a wider set of systems. These include substrates of conjugated brushes of thermoresponsive polymers such as poly[2-(2-ethoxy)ethoxyethyl vinyl ether] and poly(2-isopropyl-2-oxazoline)[1,2] as well as water-soluble polymers including poly(2-hydroxyethyl methacrylate), poly(poly(ethylene glycol), methacrylate),[30] poly(methacrylic acid),[31] and poly(ethylene glycol).[32] The approach can be used to describe functionalization by different adhesion peptides[33] such as Arg-Glu-Asp-Val (REDV).[32]

Our model incorporates two ingredients (Figure 1). First is the view that cells adhere to RGD brushes via integrin receptors binding the pendant RGD peptides. The roughly rodlike integrins are anchored to the cell membrane, and their RGD binding site is situated at their extremity, within a distance of $L_I \approx 20$ nm from the ventral cell surface.[34,35] The second ingredient concerns cell−brush interactions. An adhering cell presents an impenetrable ventral membrane to the underlying brush. The span of a typical cell, 10−60 μm, is much larger than the brush height, $h(T)$, irrespective of T and the brush swelling degree. Accordingly, a cell is similar to a large colloidal particle in that it approaches the grafting surface by compressing the brush.[36,37] However, brush confinement upon adhesion is not inevitable. For n-RGD brushes, the compression is significant only when the RGDs are situated within a distance larger than L_I from the edge of the unperturbed brush, that is, when $h(T) - \langle z\rangle_n(T) > L_I$ where $\langle z\rangle_n$ is the average equilibrium altitude of a n-RGD group in an unperturbed brush. The fulfillment of this condition depends on T, n, N, and Σ and underlies our discussion of n-RGD brush design and its extension to the ran-RGD case. Within our model, brush confinement by the adhering cells plays a double role (Figure 1): (i) Cells adhere to RGDs within an ≈20 nm region from the brush outer edge in order to avoid brush confinement and the associated disjoining pressure. The number of accessible RGD depends on the swelling state of the brush and thus on T. Since $h(T_L) \gg h(37\ °C)$ (Figure 2), the fraction of accessible RGDs is strongly reduced upon cooling. (ii) The detachment of cells adhering at $T = 37$ °C upon cooling to $T_L < T_{LCST}$ is driven by a disjoining force due to brush confinement by the anchored ventral membrane. It arises because the cells initially retain the integrin−RGD bonds formed at 37 °C. The resulting disjoining pressure places these bonds under tension, thus accelerating their dissociation according to Bell's law.[38,39] For n-RGD brushes, it is helpful to distinguish between three regimes: (i) n-RGDs at $n = N$ will favor adhesion but repress detachment because typically $h(T) - \langle z\rangle_n(T) \ll L_I$ irrespective of T. (ii) n-RGDs placed at $n \approx 1$ will promote adhesion provided $h(37\ °C) \lesssim 20$ nm and enable efficient detachment at $T_L < T_{LCST}$

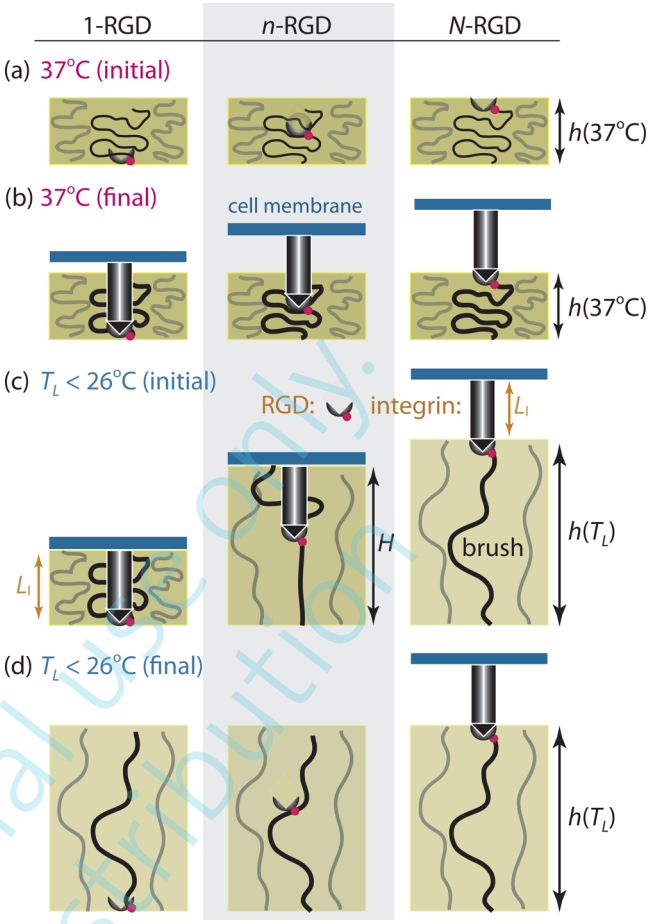

Figure 1. Schematic view of a n-RGD brush ($n = 1$, $1 \ll n \ll N$, and $n = N$) interacting with an integrin anchored to a cellular membrane illustrating the situation for cell adhesion at 37 °C, when the brush is collapsed, and cell detachment from the swollen brush at $T_L < T_{LCST}$. At 37 °C, the n-RGD equilibrium heights (a) are unperturbed by adhering cells because the integrins bind n-RGD accessible with no brush confinement (b). Upon cooling to T_L, the brush swells while the cells retain the integrin−RGD bonds formed at 37 °C. The resulting brush confinement depends on n (c). There is no confinement for $n = N$, and the confinement is maximal for $n = 1$. At intermediate n's the confinement is reduced by the compliance of the tethers. The confinement degree determines the disjoining force on the cell, thus deciding its detachment (d). For $n = N$, there is no detachment and the N-RGD are available to promote cell adhesion at both 37 °C and T_L.

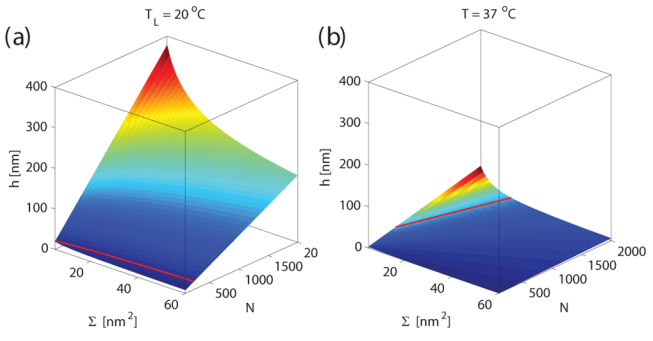

Figure 2. Unconfined brush height $h(\Sigma,N)$ for (a) $T_L = 20$ °C and (b) $T = 37$ °C (Table 1). The $h = L_I = 20$ nm contour is depicted by a red line.

dx.doi.org/10.1021/la303443t | Langmuir 2012, 28, 16623−16637

when $h(T_L) \gg 20$ nm (Figure 2). (iii) For intermediate situations, $1 \ll n \ll N$, it is necessary to allow for the compliance of the tethers anchoring the n-RGDs to the grafting surface. For randomly placed RGDs in ran-RGD brushes, there is always a significant fraction of high n RGDs leading to reduced detachment efficiency.

The 1-RGD brush (Figure 1) is similar to PNIPAM brush substrates utilizing serum containing medium when ECM proteins undergo primary adsorption at the grafting surface.[37] However, the two systems differ in the mechanism controlling the surface density of integrin ligands. The amount of physically adsorbed VN and FN in the "serum case" is sensitive to Σ, N, T, and the nature of the grafting surface. In contrast, the RGD density in RGD brushes is set by the synthesis. While our analysis concerns n-RGD and ran-RGD brushes, the formulation of the problem drew on experimental results on RGD conjugated e-b hydrogels.[24−27] Our results are qualitatively applicable to this system to the extent they may be considered as weakly cross-linked brushes. With this caveat our model allows to rationalize experimental observations concerning RGD conjugated e-b hydrogels and we comment on this issue in the Discussion.

Our analysis invokes the height distribution of the nth monomers, thus requiring a self-consistent field (SCF) theory approach. The analytical version of the SCF theory enables an efficient exploration of the Σ, N effects (Appendix A).[28,40] To allow for the phase diagram of PNIPAM and its effects on the T dependence of the brush structure, we use a SCF theory[41] incorporating the empirical mixing free energy of PNIPAM solutions proposed by Afroze, Nies, and Berghmans (ANB)[42] (Appendix B). The ANB free energy reproduces the phase boundaries of PNIPAM, and its combination with SCF theory yields brush concentration profiles in semiquantitative agreement with experiments.[43−46] In implementing the theory, we exclude the 26 °C < T < 30 °C range where PNIPAM brushes undergo a vertical phase separation and the SCF equations require numerical solution. The chosen T range, T > 30 °C and T_L < 26 °C, includes the temperatures utilized in cell sheet engineering. As we will demonstrate, it also affords the advantages of quantitative analytical approximations for the monomer volume fraction at altitude z, $\phi(z)$, and all related properties (Table 1). Within this model, the brush is collapsed at $T \simeq 37$ °C and its properties are well described by the asymptotic poor solvent SCF results. The asymptotic good solvent SCF theory applies when T_L < 26 °C and the brush is swollen (Appendix B). Since RGD peptides are relatively small molecules, and only a minority of the monomers is functionalized by RGDs, we further assume that the brush structure is unmodified by the conjugated RGDs. At this preliminary stage, we ignore for simplicity the size differences between conjugated and nonconjugated monomers. The analysis presented is preliminary and aims to identify qualitative traits. The numerical factors arising from SCF normalization conditions and the ANB free energy are retained to ensure sensible implementation of the theory but do not suggest a level of accuracy.

Table 1. Asymptotic Good and Poor Solvent SCF Results Used to Approximate the Full ANB[42] PNIPAM SCF Model at T = 37°C and T_L < 26°C < T_{LCST}[a]

	PNIPAM (T = 37 °C) asymptotic poor	PNIPAM (T_L < 26 °C) asymptotic good $\hat{\nu} \simeq 1.5 - 0.1 \times (T_L - 20\ °C)$
h	$(a^2/\Sigma)Na/\phi_0$	$(8p\hat{\nu}/\pi^2)^{1/3}(a^2/\Sigma)^{1/3}Na$
ϕ_0	0.7	$(3/2)(a^2/\Sigma)Na/h$
$\phi(z)$	ϕ_0	$\phi_0[1 - (z/h)^2]$
$g(z_N)$	$(z_N/h)(h^2 - z_N^2)^{-1/2}$	$(3z_N/h^3)(h^2 - z_N^2)^{1/2}$
$\langle z \rangle$	$h/2$	$3h/8$
$\langle z^2 \rangle$	$h^2/3$	$h^2/5$
h_n	$h \sin(\pi n/2N)$	$h \sin(\pi n/2N)$
$\langle z \rangle_n$	$\pi h_n/4$	$3\pi h_n/16$
$\phi_n(z)$	$(a^3/\Sigma)(h/h_n)g(zh/h_n)$	$(a^3/\Sigma)(h/h_n)g(zh/h_n)$

[a]For PNIPAM, we utilize[37] p = 1, a = 0.5 nm. Details leading to the calculation of all table entries are provided in the Appendices.

Our discussion involves three parts. First, in section 2, we address brush design to promote cell adhesion. To this end, we consider the accessibility of the RGDs to cells as determined by the properties of unperturbed n-RGD and ran-RGD PNIPAM brushes. In particular, we quantify the T dependent accessibility of n-RGD from the volume fraction profiles of the nth monomers, $\phi_n(z)$, specifying their height distribution between z = 0 at the grafting surface and a n-dependent maximal altitude $h_n(T) \leq h(T)$. The $\phi_n(z)$ profiles define two characteristic n's, n_h and n_m, such that $n > n_h$ ensures $h_n > h - L_I$ and $n > n_m$ assures $\langle z \rangle_n > h - L_I$. n_h and n_m provide, as shall see, a criterion for choosing n so as to ensure accessibility of n-RGDs to adhering cells with negligible brush compression. Similarly, we obtain the fraction of accessible RGDs in ran-RGD brushes when the RGDs concentration profile is proportional to $\phi(z)$. Next, in section 3, we consider brush design to promote detachment of cells cultured at 37 °C upon cooling to T_L < 26 °C. Within our model, the detachment at T_L is driven by a disjoining force f_{cell} arising from the confinement of the swollen brush by adhering cells that initially maintain integrin−RGD bonds formed at 37 °C. It is due to the accelerated dissociation of tensioned integrin−RGD bonds and metabolically active processes it triggers. The estimation of f_{cell} is sensitive to the absolute height map of the ventral membrane. However, the effect of the n-RGD tether compliance on f_{cell} is discernible from a simple model considering the cell as a planar piston. The piston is anchored to the grafting surface via integrin−n-RGD bonds, and its altitude is set by the balance of the disjoining force and the restoring elastic force of the stretched n-RGD tethers. The mechanical equilibrium specifies the initial tension on the integrin-n-RGD bonds, thus determining their initial dissociation rate. This analysis identifies a characteristic n of a fully stretched tether reaching the $h - L_I$ zone denoted as $n_s \equiv (h - L_I)/a$, such that efficient harvesting at T_L is attained for $n < n_s(T_L)$. In turn, n_s serves as a basis for our discussion of detachment efficiency in n-RGD and ran-RGD brushes. The planar piston approximation overlooks upward bulges in the ventral membrane. It thus overestimates the brush confinement and yields an upper bound for f_{cell}. To obtain a more realistic estimate of f_{cell}, we utilize a ventral height profile based on the data reported by Iwanaga, Braun, and Fromherz (IBF)[47] for fibroblasts adhering to FN coated silica. To judge the relevance of the mechanism, we propose it is necessary to estimate the effect of f_{cell} on cell detachment. The initial detachment rate may be attributed to the accelerated dissociation of the tensioned integrin−n-RGD bonds. To quantify this effect, in the absence of explicit force spectroscopy data on this bond, we will utilize the force dependent integrin−FN dissociation rate as measured and modeled by Li, Redick, Erickson, and Moy (LREM).[48] This rough approximation is based on the observation that the FN−integrin bond involves a RGD

domain in FN though it does not allow for the contribution of other FN peptide sequences participating in the bond. The full analysis of the detachment cannot be implemented for ran-RGD brushes where the tether extension is inherently nonuniform. It is however possible to characterize qualitative aspects of this case by considering the fraction of strongly tensioned integrin−RGD bonds with $n < n_s$. Finally, in section 4, we combine the results of the previous sections to obtain design guidelines for thermoresponsive RGD conjugated PNIPAM brush substrates enabling adhesion at 37 °C and efficient detachment at $T_L < 26$ °C. The comparison between the *n*-RGD and ran-RGD cases emphasizes the utility of controlling the RGD altitude within the brush. Existing experimental results concerning RGD conjugated e-b hydrogels are summarized in the Discussion and Conclusions highlighting the relationship to the formulation of our model and possible future experiments. We also comment on the interpretation of cell culture studies on RGD e-b hydrogels within our model.

2. RGD ACCESSIBILITY AND CELL ADHESION

Cells adhering to impenetrable surfaces develop focal adhesions when the RGD surface density exceeds a certain threshold, σ_{crit}. Estimates of σ_{crit} vary in the range of[49] 60 to[50] 300 RGDs/μm^2. RGD conjugated brushes are however penetrable, and it is helpful to distinguish between the total RGD surface density σ_{total} and the surface density of accessible RGDs, $\sigma_{accessible}$. Cell adhesion requires $\sigma_{accessible} > \sigma_{crit}$ rather than $\sigma_{total} > \sigma_{crit}$. In contrast to σ_{total}, $\sigma_{accessible}$ is sensitive to $\phi(z)$, T and n that determine the fraction ψ of RGDs within a distance $L_I \approx 20$ nm from the outer edge of the unperturbed brush.

The accessibility of the *n*-RGDs is determined by the concentration profile of the *n*th monomers in the unperturbed brush as it varies with the altitude z (Appendix A and Figure 3). For thin layers $h \le L_I$, all RGDs are accessible. We thus focus on the $h \ge L_I$ case when the number of accessible *n*-RGD per unit area is

$$\sigma_{accessible}(n) = \frac{\alpha_{RGD}}{a^3}\int_{h-L_I}^{h}\phi_n(z)\,dz \tag{1}$$

where α_{RGD} is the fraction of functionalized chains and $\phi_n(z)$ is the volume fraction profile of the *n*th monomers. The total number of *n*-RGDs is $\sigma_{total} = \alpha_{RGD}/\Sigma$, and the accessible fraction of *n*-RGDs is thus

$$\psi(n) = \frac{\sigma_{accessible}(n)}{\sigma_{total}(n)} = \frac{\Sigma}{a^3}\int_{h-L_I}^{h}\phi_n(z)\,dz \tag{2}$$

For the T range considered, the analytical SCF approximation applies and (Appendix C)

$$\psi(n) = \left[1 - \left(1 - \frac{L_I}{h}\right)^2 \Big/ \sin\left(\frac{n\pi}{2N}\right)\right]^{\alpha} \tag{3}$$

where $\alpha = 1/2$ for 37 °C and $\alpha = 3/2$ for $T_L < 26$ °C. Plots of $\psi(n)$ at 37 °C and T_L are qualitatively similar, that is, $\psi(n)$ decreases with increasing h and n/N. The effect of the Σ, N, and T dependence of h is evident upon considering specific values of Σ and N (Figure 4): $\psi(n) \approx 1$ at 37 °C while $\psi(n)$ at 20 °C varies in the 0−0.6 range depending on N and Σ. To explicitly bring out the effect of Σ and N, it is helpful to characterize $\psi(n)$ in terms of two features of the $\phi_n(z)$ profiles. The first one is the average position of the *n*th monomer (Appendix A)

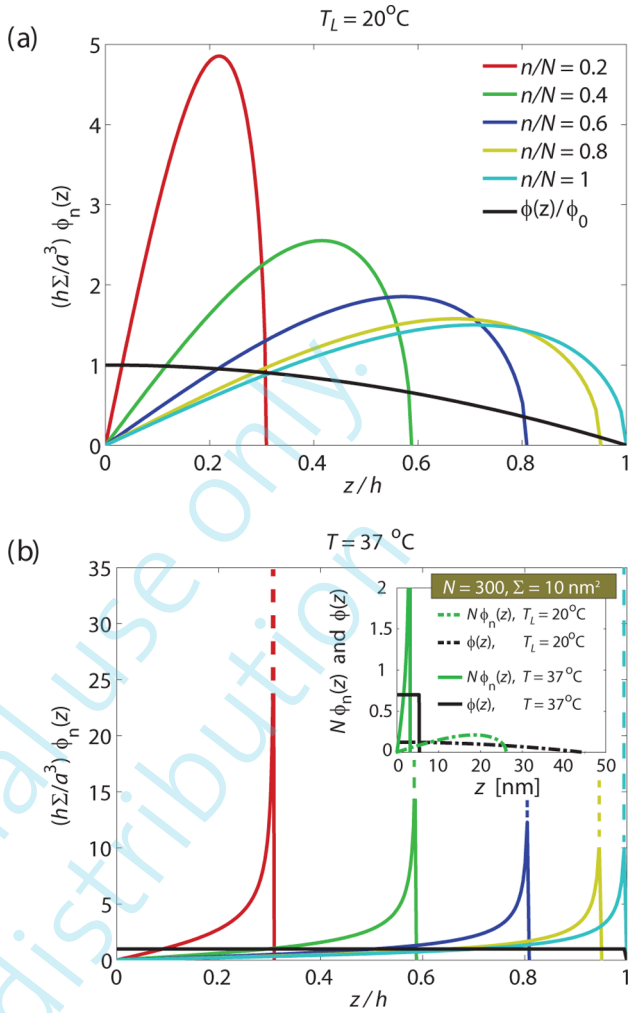

Figure 3. The distribution of the *n*th monomer $\phi_n(z)$ for (a) $T_L = 20$ °C and (b) $T = 37$ °C calculated via eq 35 with $g(z_N)$ cited in Table 1.

$$\langle z\rangle_n = \frac{\Sigma}{a^3}\int_0^h z\phi_n(z)\,dz = \frac{\pi}{2}\langle z\rangle\sin\left(\frac{n\pi}{2N}\right) \tag{4}$$

as specified in terms of n/N and the average monomer height $\langle z\rangle$ within the brush whose monomer volume fraction profile is $\phi(z)$. The second feature is the maximal height populated by the *n*th monomers, h_n (Appendix A),

$$h_n = h\sin\left(\frac{n\pi}{2N}\right) > \langle z\rangle_n \tag{5}$$

that is, $\phi_n(z) = 0$ for $h_n \le z \le h$.

In turn, the expressions for $\langle z\rangle_n$ and h_n suggest the definition of two characteristic *n*'s. The first, n_m,

$$n_m = \frac{2N}{\pi}\arcsin\left[\frac{2h}{\pi\langle z\rangle}\left(1 - \frac{L_I}{h}\right)\right] \qquad (0 \le h - L_I \le \pi\langle z\rangle/2) \tag{6}$$

delineates the accessibility in terms of the mean $\langle z\rangle_n$ such that $n > n_m$ satisfies $\langle z\rangle_n > h - L_I$. The second is similarly defined in terms of h_n

$$n_h = \frac{2N}{\pi}\arcsin\left(1 - \frac{L_I}{h}\right) < n_m \qquad (h \ge L_I) \tag{7}$$

dx.doi.org/10.1021/la303443t | *Langmuir* 2012, 28, 16623−16637

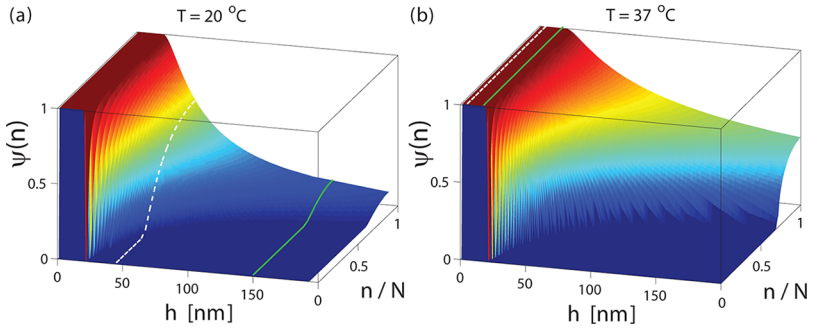

Figure 4. The fraction of accessible nth monomers, $\psi(n)$, versus h for (a) T_L = 20 °C and (b) T = 37 °C. The lines indicate $\psi(n)$ values obtained for two representative systems further investigated in Figure 6: N = 300, Σ = 10 nm^2 (white), and N = 1000, Σ = 10 nm^2 (green).

so that $n > n_h$ ensures $h_n > h - L_I$. Since $\langle z\rangle_n < h_n$ shifting $\langle z\rangle_n$ to the $h - L_I$ zone requires a higher n_m value, $n_m > n_h$. Both n_m and n_h increase with $h(T)$, indicating the effect of brush swelling on n-RGD accessibility. For $h \gg L_I$, most of the interior monomers are below the $h - L_I$ region and only the terminus region is accessible, $n_m \approx n_h \approx N$. Maximal accessibility is attained at $h \leq L_I$ when $n_m = n_h = 0$. Since $n_m > n_h$, the more stringent design criterion for choosing n/N for n-RGD peptides so as to promote cell adhesion is $n > n_m$.

Equations 6 and 7 are independent of the interaction term of the free energy invoked to describe the brush and formulate the SCF theory. In particular, they apply to "classical" brushes described by the Flory mixing free energy and to PNIPAM brushes as modeled using the ANB free energy. Furthermore, these relationships hold irrespective of T and the swelling degree of the brush be it collapsed or swollen. Efficient utilization of these equations to explore the N, Σ, and T dependence of n_m and n_h is facilitated by closed form analytical expressions for $h = h(N,\Sigma,T)$ (Table 1). We thus limit the analysis to temperatures relevant to cell sheet engineering, $T_L <$ 26 and 37 °C, where $\phi(z)$ is well approximated by the asymptotic good solvent ($T_L <$ 26 °C) and poor solvent SCF expressions (Appendix B). At 37 °C, when $\phi(z) \approx \phi_0$ (37 °C) $\simeq$ 0.7

$$n_m\,(37°\mathrm{C}) = \frac{2N}{\pi}\arcsin\left[\frac{4}{\pi}\left(1 - 0.7\frac{L_I}{Na}\frac{\Sigma}{a^2}\right)\right] \quad (a^2 \ll \Sigma \lesssim N^{2/3}a^2) \tag{8}$$

while at T_L

$$n_m(T_L) = \frac{2N}{\pi}\arcsin\left\{\frac{16}{3\pi}\left[1 - \left(\frac{\pi^2}{8p\hat{v}}\frac{\Sigma}{a^2}\right)^{1/3}\frac{L_I}{Na}\right]\right\} \quad (a^2 \ll \Sigma \lesssim N^{6/5}a^2) \tag{9}$$

where the dimensionless second virial coefficient (Appendix B) may be conveniently expressed as $\hat{v} \simeq 1.5{-}0.1\ (T - 20\ °\mathrm{C})$. The T dependence of n-RGD accessibility is evident from plots of n_h/N and n_m/N versus Σ and N for the experimentally explored range of 10 nm$^2 \leq \Sigma \leq$ 50 nm^2 and 200 < N < 2000 (Figure 5). At 37 °C, when the brush is collapsed, most Σ and N yield h (37 °C) $\leq L_I$ thus leading to n_h (37 °C) $\approx n_m$ (37 °C) $\approx$ 0, signaling complete accessibility. In contrast, the RGD accessibility of swollen brush at T_L is strongly reduced with $n_m/N > n_h/N \gg 0$ for most Σ and N values.

Similar analysis can be carried out for the ran-RGD scenario where the RGD peptides are randomly placed along the chains.

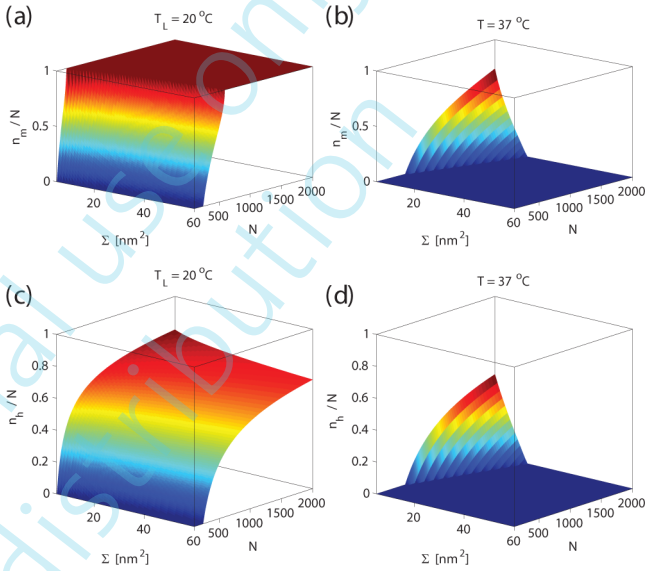

Figure 5. Characteristic n's (a,b) n_m/N and (c,d) n_h/N versus Σ and N for (a,c) T = 20 °C and (b,d) 37 °C, calculated via eqs 6, 7 and Table 1.

In this case, the brush is characterized by Σ, N and by the fraction x_{RGD} of monomers with pendant RGD such that $\phi_{RGD}(z) = x_{RGD}\phi(z)$. When $h < L_I$, all RGDs are accessible, while for $h > L_I$ the number of accessible RGDs per unit area is

$$\sigma_{\text{accessible}}^{\text{random}} = \frac{x_{RGD}}{a^3}\int_{h-L_I}^{h}\phi(z)dz \tag{10}$$

The total number of RGDs per unit area is $\sigma_{\text{total}}^{\text{random}} = x_{RGD}N/\Sigma$ and the fraction of accessible RGDs, ψ_{random}, is thus

$$\psi_{\text{random}} = \frac{\sigma_{\text{accessible}}^{\text{random}}}{\sigma_{\text{total}}^{\text{random}}} = \frac{\Sigma}{Na^3}\int_{z_{low}}^{h}\phi(z)\,dz \tag{11}$$

leading, invoking Table 1, to

$$\psi_{\text{random}}\,(37°\mathrm{C}) = \frac{L_I}{h\,(37°\mathrm{C})} = 0.7\frac{L_I}{Na}\frac{\Sigma}{a^2} \tag{12}$$

and

$$\psi_{\text{random}}(T_L) = \frac{3}{2}\left[\frac{L_I}{h(T_L)}\right]^2\left[1 - \frac{1}{3}\frac{L_I}{h(T_L)}\right] \tag{13}$$

As in the n-RGD case, the ran-RGD accessibility depends strongly on the swelling degree as determined by T. At T = 37 °C, when the brush is collapsed, h (37 °C) < L_I is realized over

dx.doi.org/10.1021/la303443t | Langmuir 2012, 28, 16623−16637

a wide range of Σ and N leading to $\psi_{random} \approx 1$. Brush swelling upon lowering T below T_{LCST} reduces ψ_{random}. This effect is small for $N \lesssim 200$ when $h(T_L) \lesssim L_I$ and increases significantly for $N > 500$.

Overall, thermoresponsive PNIPAM brush substrates must satisfy two conditions: (i) $\sigma_{accessible}$ (37 °C) > σ_{crit} to promote adhesion and proliferation of seeded cells at 37 °C. (ii) $\sigma_{accessible}(T_L) < \sigma_{crit}$ to repress cell adhesion at T_L so as to permit harvesting of the cultured cells. Within our model, $\sigma_{accessible} = \psi\sigma_{total}$ and $\sigma_{total} > \sigma_{crit}$ is thus a necessary but insufficient design guideline. To ensure functionality, one must also require ψ(37 °C)$\sigma_{total} > \sigma_{crit}$ and $\psi(T_L)\sigma_{total} < \sigma_{crit}$. As we shall discuss later, the "nonadhesion" at T_L requirement can be replaced by a more stringent condition assuring efficient detachment.

3. THE EFFECT OF *n* ON CELL DETACHMENT

Our discussion of *n*-RGD and ran-RGD accessibility utilized results concerning unperturbed brushes. In contrast brush confinement is crucial to our model of cell detachment from RGD brushes. Adhering cells cultured at 37 °C spread and form integrin−ligand bonds. A typical projected area of an adhering cell is $A_{proj} \approx 2000\ \mu m^2$ while estimates of the number of integrin−ligands bonds, m_0, vary in the 10^4−10^5 range.[37,49,50] Importantly, for typical PNIPAM brushes, 10 $nm^2 \leq \Sigma \leq 50$ nm^2 and only a minority of the RGDs are expected to be bound, that is, $A_{proj}/m_0 \gg \Sigma$. Within our model, the cells cultured at 37 °C form m_0 integrin−RGD bonds with no brush confinement. The cells initially retain these bonds upon cooling to T_L. This constraint on the ventral cell membrane gives rise to confinement of the now swollen brush. The resulting disjoining pressure is opposed by the elasticity of the tethers binding the RGDs to the substrate. The tethers stretch outward so as to lower the confinement of the brush. The tether compliance thus reduces the tension on the integrin−RGD bonds with corresponding decrease in their dissociation rate. A full description of the detachment process should account for the kinetics of brush swelling and the dynamics of the cells. Such complete discussion is premature and currently impractical. A simpler analysis is however sufficient to identify qualitative features and suggest design guidelines for the case of *n*-RGD brushes. We will thus first analyze *n*-RGD brushes and later utilize the results in considering ran-RGD brushes. To this end, we limit the discussion to the initial integrin−*n*-RGD dissociation following a temperature quench from 37 °C to T_L < 26 °C. We further assume that the brush relaxation is fast in comparison to the membrane response. For simplicity, we initially approximate the cell ventral membrane as a planar piston placed at height $H \simeq z_n^* + L_I$ above the grafting surface. z_n^* specifies the yet to be determined position of the m_0 bound *n*-RGDs in mechanical equilibrium reflecting the balance of the disjoining force acting on the cell at T_L and the elastic restoring force of the m_0 stretched tethers. Since $A_{proj} \gg \Sigma$, the disjoining pressure $P(H)$ acting on the cell when $H < h(T_L)$ is specified by the planar piston form of a brush in an asymptotic good solvent[28,40,51]

$$P(H) = P_0\left(\frac{h}{H} - \frac{H^2}{h^2}\right)^2, \quad P_0 = \frac{\pi^{4/3}}{12}\left(\frac{\hat{v}}{p}\right)^{1/3}\left(\frac{a^2}{\Sigma}\right)^{4/3}\frac{k_B T_L}{a^3} \tag{14}$$

where $\Pi_0 a^3/k_B T = v\hat{\phi}_0^2$ is specified by $P_0 = 4\Pi_0/9$ upon using ϕ_0 at T_L (Table 1). The disjoining force acting on the cell within this approximation is $f_{cell} = A_{proj}P(H)$. f_{cell} perturbs the m_0 chains bearing integrin bound *n*-RGDs. While the configuration of the whole chain is affected, the leading effect is stretching of the tethers joining the *n*-RGDs to the surface. Finite extensibility is expected to play a role for small *n*'s, and we thus describe the elasticity of the strongly stretched tethers using the wormlike chain (WLC) model in the form[52]

$$f_{WLC}(z_n) = \frac{k_B T}{l_p}\left[\frac{z_n}{na} + \frac{1}{4(1 - z_n/na)^2} - \frac{1}{4}\right] \tag{15}$$

where $l_p \approx pa$ is the persistence length of the polymer and p is the number of monomers in a persistent segment. $f_{WLC}(z_n)$ accounts well for the strong extension behavior observed in AFM experiments where individual chains from a polymer brush were strongly stretched outward.[53] However, it predicts $f_{WLC}(z_n) = 0$ at $z_n = 0$, while for an unperturbed brush the *n*th monomer experiences no average net force at $\langle z\rangle_n > 0$. To address this problem, we utilize the simplest elastic force law reducing to $f_{WLC}(z_n)$ for strong extensions while vanishing at $z_n = \langle z\rangle_n$

$$f_{elastic}(z_n) = f_{WLC}(z_n) - f_{WLC}(\langle z\rangle_n) \tag{16}$$

This $f_{elastic}(z_n)$ remains a rough approximation. A rigorous treatment should explicitly allow for different contributions reflecting tether interactions, tether stretching, and their counterparts for the nonstretched chain segment comprising of monomers $n + 1$ to N. It should also allow for nonuniform chain extension. With these caveats, eq 16 captures the leading features of both weak and strong extension behavior. Note also that eq 16 partially allows for the effect of monomer−monomer interactions by imposing $f_{elastic}(\langle z\rangle_n) = 0$. The derivation $f_{WLC}(z_n)$ assumes a long chain and it is not strictly speaking applicable to short tethers of $n \gtrsim 1$. However, in the numerical implementation, we utilize $f_{elastic}(z_n)$ for the full $1 \leq n \leq N$ range since this prescription captures the correct behavior, that is, $n = 1$ acts as a rigid spacer of length a.

The mechanical equilibrium established at the instant of the temperature quench is specified by the force balance

$$m_0 f_{elastic}(z_n^*) = A_{proj}P(z_n^* + L_I) \tag{17}$$

determining z_n^* and the corresponding tether tension $f_{tether}^*(n) = f_{elastic}(z_n^*)$. The extension of a single tether is thus balanced by the compression of $A_{proj}/m_0\Sigma \gg 1$ chains. As a result the system tends to favor stretching of the tethers over confinement of the brush. Two characteristic *n*'s play a role in determining z_n^* and $f_{tether}^*(n)$. One is n_m introduced earlier. The tether length is weakly affected when $n \gtrsim n_m$ because the bound *n*-RGDs are within the $h - L_I$ zone and the adhering cells do not compress the brush. The second characteristic *n* is $n_s = (h - L_I)/a$, the minimal *n* of a fully stretched tether reaching the $h - L_I$ zone. While the following considerations concerning the force balance are valid for any T, our discussion concerns $T_L < T_{LCST}$ and thus involves h, n_s, n_m, $\langle z\rangle_n$, and P at T_L (Table 1, eqs 6, 9 and 14).

Tethers of $n \ll n_s$ minimize the brush compression by strong stretching to $z_n^* \approx na$, and $f_{tether}^*(n)$ is determined by the disjoining pressure at $H = na + L_I$. At intermediate $n_s \ll n \leq n_m$, the tethers stretch so that the ventral membrane is at $H \approx h$ and $f_{tether}^*(n)$ is determined by $f_{elastic}(h - L_I)$. In the vicinity of n_s the nonlinear term in $f_{elastic} \approx f_{WLC}$ is balanced by the weak compression of $A_{proj}/m_0\Sigma \gg 1$ chains leading to $z_{n_s}^* < n_s a$ (Appendix D). The z_n^* regimes at T_L are thus

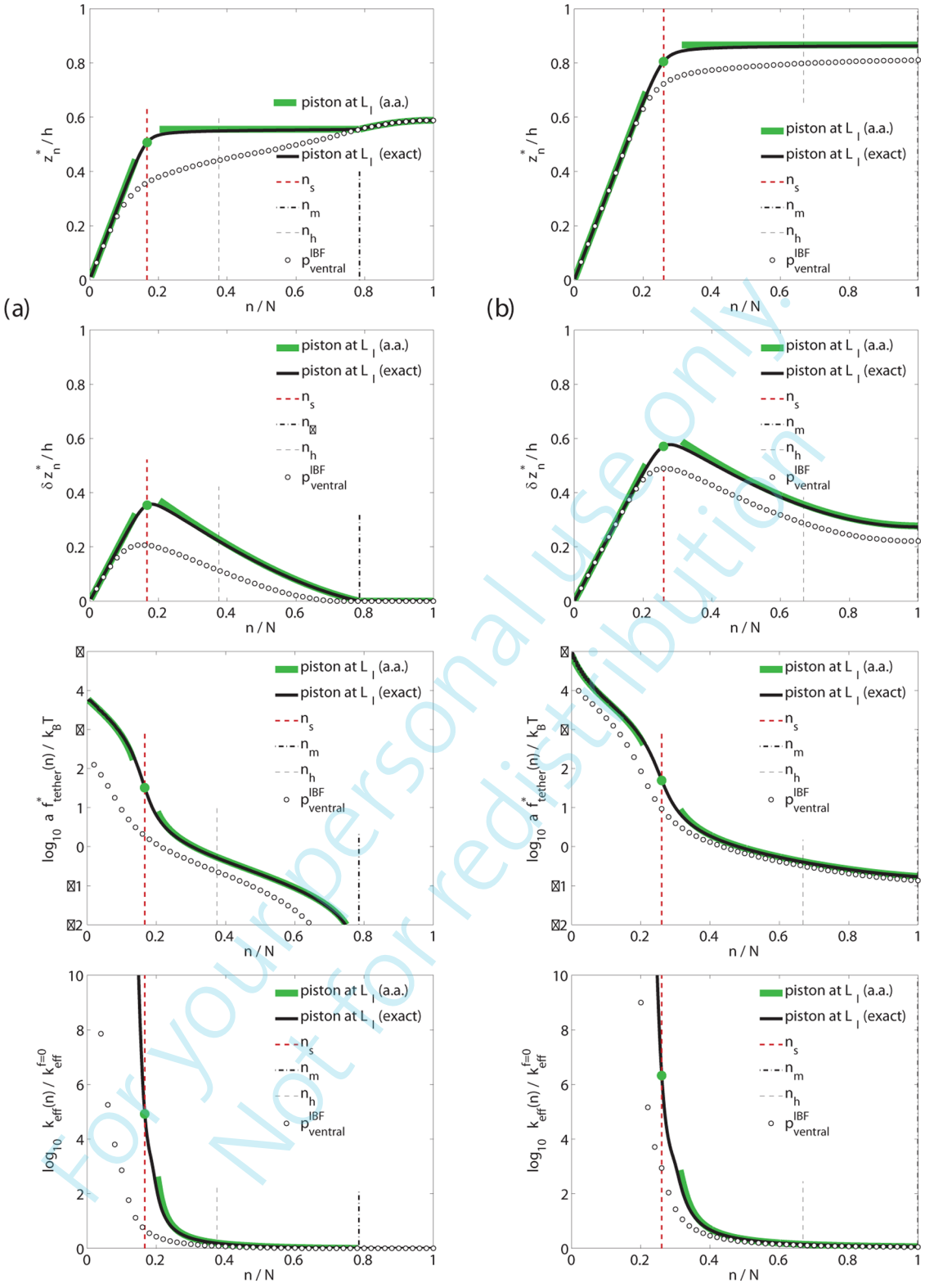

Figure 6. The characteristics of the initial mechanical equilibrium z_n^*, $\delta z_n^* = z_n^* - \langle z \rangle_n$, $f_{\text{tether}}^*(n)$, and the corresponding detachment rate $k_{\text{eff}}(n)$ versus n/N at $T_L = 20$ °C for (a) $N = 300$, $\Sigma = 10$ nm^2, and (b) $N = 1000$, $\Sigma = 10$ nm^2. Obtained by numerically solving the force balance $m_0 f_{\text{elastic}}(z_n^*) = f_{\text{cell}}(z_n^*)$ (eq 17) with $m_0 = 5 \times 10^4$ for both the planar piston at L_I (exact) and the IBF height profile ($p_{\text{ventral}}^{\text{IBF}}$, Figure 7), as well as with the analytic approximations eqs 18 and 19 (a.a). Also shown is the location of the characteristic n's.

dx.doi.org/10.1021/la303443t | *Langmuir* 2012, 28, 16623−16637

$$z_n^* \approx \begin{cases} na, & n \ll n_s \quad (a) \\ z_{n_s}^* = n_s a - \dfrac{(n_s a)^{1/2} h^{1/2}}{(36C)^{1/4}}, & n \approx n_s \quad (b) \\ n_s a \equiv h - L_I, & n_s \ll n \le n_m \quad (c) \\ \langle z \rangle_n, & n > n_m \quad (d) \end{cases} \tag{18}$$

where $C \equiv P_0 A_{proj} a / m_0 k_B T$, and only case (b) is specific to T_L. The stretching behavior is clearly manifested in the variation of the difference $\delta z_n = z_n^* - \langle z \rangle_n$ with n. $\delta z_1 = 0$ because the tether is not extensible while δz_N is also small because the terminal monomers are anyhow localized at the vicinity of the edge. δz_n exhibits a maximum at the vicinity of n_s. It arises because for $n \ll n_s$, $\delta z_n = na - \langle z \rangle_n$ increases with n since $\langle z \rangle_n \sim \sin(n\pi/2N)$, while for $n \gg n_s$, $\delta z_n = h - L_I - \langle z \rangle_n$ and thus decreases with increasing n. The corresponding $f_{tether}^*(n)$ are

$$f_{tether}^*(n) \approx \begin{cases} A_{proj} P(na + L_I)/m_0, & n \ll n_s \quad (a) \\ \dfrac{3}{2}(Cn_s)^{1/2} k_B T/h, & n \approx n_s \quad (b) \\ f_{elastic}(h - L_I), & n_s \ll n \le n_m \quad (c) \\ 0, & n > n_m \quad (d) \end{cases} \tag{19}$$

Note that z_n^* as given by eqs 18(a) and (c) match at $n = n_s$ yielding $z_{n_s}^* = n_s a$. In contrast eqs 19(a) and (c) lead to very different $f_{tether}^*(n)$ at $n = n_s$, that is, eq 19(a) yields $f_{tether}^*(n_s) \sim P(n_s a) = 0$ while eq 19(c) leads to $f_{tether}^*(n_s) \approx f_{elastic}(n_s a) = \infty$. There is however no discrepancy, because eqs 19(a) and (c) do not apply at $n = n_s$. These considerations highlight the usefulness of the exact result eq 19(b) at $n = n_s$, as derived for T_L (Appendix D). We finally stress that the regime in eq 19(d) is attainable only for $n_m < N$. z_n^* and $f_{tether}^*(n)$, as obtained by numerical solution of the mechanical equilibrium condition, confirm the validity of eqs 18 and 19 (Figure 6).

Approximating the ventral membrane as a planar piston identifies the leading regimes in terms of $n_s(T_L)$ and $n_m(T_L)$. It however overestimates the brush compression and the associated f_{cell}. This is because the ventral membrane varies in height with regions of close proximity to the substrate, associated with focal adhesions, and upward bulges. The planar piston approximation ignores the upward bulges where the confinement is weaker. The disjoining pressure and the resulting f_{cell} should be determined from the ventral membrane absolute height map as compared to the equilibrium brush height, $h(T)$. The Derjaguin approximation is applicable when the lateral variation of the height is slow: The disjoining force on a cell, f_{cell}, is then obtained by summing up the contributions due to area elements of certain H assuming that each area element locally imposes the disjoining pressure $P(H)$ associated with confinement by a planar piston at altitude H. Accordingly, for a cell with a projected area A_{proj}

$$f_{cell}(z_n) = A_{proj} \int_0^\infty p_{ventral}(H, z_n)\, P(H)\, dH \tag{20}$$

where $p_{ventral}(H,z_n)$ is the height probability distribution density of the ventral membrane when the n-RGD is at altitude z_n. Note that eq 20 accounts only for compressed regions with $H < h(T)$ because $P(H)$ vanishes for $H \ge h$. Similarly, $p_{ventral}(H,z_n)$ may vanish at low H, thus setting the lower bound of the H range contributing to f_{cell}.

Ventral height maps of cells cultured on PNIPAM brushes or hydrogels are yet to be measured. To illustrate the effect of $p_{ventral}(H,z_n)$ on f_{cell}, we thus utilize results concerning cells adhering to FN coated surface as reported by IBF.[47] However, the IBF data reflects a contribution due to an adsorbed FN layer of thickness $d \approx 5$ nm and cannot be utilized in their original form. To circumvent this difficulty, we argue that the RGDs, to be accessible, are located at the outer edge of the FN layer, that is, we subtract $d \approx 5$ nm from the IBF heights and obtain the distribution $p_{ventral}^{IBF}(\Delta H)$ of the ventral membrane

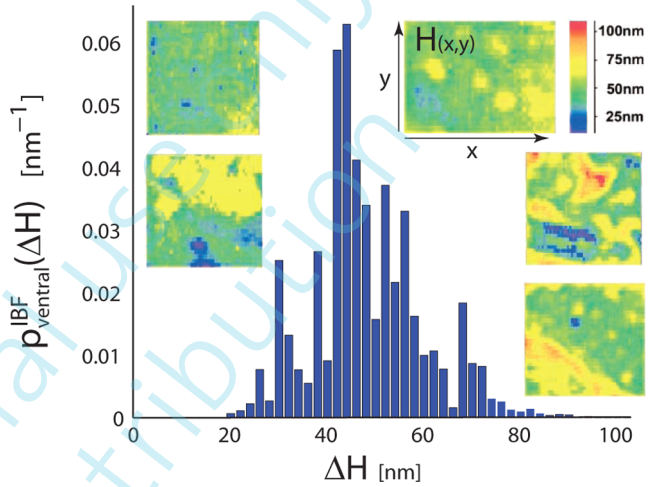

Figure 7. Ventral height map $p_{ventral}^{IBF}(\Delta H)$ versus ΔH extracted from data[47] shown in the insets.

height with respect to the RGD, ΔH (Figure 7). $p_{ventral}^{IBF}(\Delta H)$ specifies f_{cell} assuming $H = z_n + \Delta H$ or

$$f_{cell}^{IBF}(z_n) = A_{proj} \int_0^\infty p_{ventral}^{IBF}(H - z_n)\, P(H)\, dH \tag{21}$$

The initial mechanical equilibrium condition $m_0 f_{elastic}(z_n^*) = f_{cell}^{IBF}(z_n^*)$ as obtained using the IBF data is qualitatively similar to the one obtained from the planar piston approximation but yields, as expected, lower $f_{tether}^{*IBF}(n)$ (Figure 6). The deviations of $f_{tether}^{*IBF}(n)$ from the planar piston approximation diminish with increasing $h(T_L)$ because the width of $p_{ventral}^{IBF}(\Delta H)$ is small in comparison to $h(T_L)$ of extended brushes and $P(H)$ is a unique function of H/h.

The main thrust of this section concerned the estimation of $f_{tether}^*(n)$ and z_n^*; however, an additional step is necessary to explore the relevance of the model to cell harvesting at T_L. While f_{cell} is the proposed driving force for cell detachment, it is not directly observable in cell culture experiments. It is thus necessary to estimate the effect of f_{cell} on the detachment rate. To this end, we consider the initial dissociation rate of the m_0 tensioned integrin−n-RGD bonds, at the instant of the T quench. The initial f_{cell} is equally partitioned among m_0 bonds loaded in parallel.[39] In this situation, the effective rate constant of dissociation for a single barrier energy landscape is given by $k_{eff} = m_0 k_0 \exp[f_{tether}^*(n) x_b / k_B T]$, where x_b is the position of the barrier as measured from the minimum of the well and $k_0 = \tau^{-1} \exp(-E_b/k_B T)$ is the dissociation rate constant of the unloaded bond. k_0 is defined in terms of the height of the activation barrier, E_b, and a characteristic attempt time τ. The exp-

dx.doi.org/10.1021/la303443t | Langmuir 2012, 28, 16623−16637

$[f^*_{tether}(n)x_b/k_BT]$ factor, reflecting Bell's law,[38] accounts for the effect of the tension on the barrier height. The effect of the tether compliance is incorporated via z_n^* and the corresponding $f^*_{tether}(n)$. It is qualitatively similar to the effect considered by Evans and Ritchie[54] in their analysis of force spectroscopy of weak bonds linked to a substrate by flexible polymer chains. The m_0 prefactor allows for the number of possible ways of breaking a bond. To our knowledge, the force spectroscopy of integrin−RGD bonds remains to be explored. To circumvent the lack of data concerning this system, we utilize force spectroscopy results concerning integrin−FN bonds. The integrin−FN bonds involve the RGD containing domain of FN, thus suggesting similarity. The room temperature force spectroscopy measurements of LREM[48] suggest that the integrin−FN bond energy landscape involves two barriers at $x_b(1) \approx 0.9$ Å and $x_b(2) \approx 4.2$ Å with barrier heights of $E_b(1) = 11.7k_BT$ and $E_b(2) = 17.3k_BT$ as measured with respect to the fundamental minimum of the potential well. The corresponding dissociation energy is $18.8k_BT$. Their results for single bond dissociation are described by $k_{eff}^{-1} = \Sigma_{l=1}^{2} k_0^{-1}(l) \exp[-fx_b(l)/k_BT]$ with room temperature values of $k_0(1) = \tau^{-1} \exp(-E_b(1)/k_BT) = 33.5\ s^{-1}$ and $k_0(2) = \tau^{-1} \exp(-E_b(2)/k_BT) = 0.13\ s^{-1}$. The LERM experiment involves varying the applied force at a fixed T so that $k_0(1)$ and $k_0(2)$ are constants. In contrast, in our situation f_{cell} is tuned by lowering T, thus affecting both the k_0 and the $\exp(fx_b/k_BT)$ factors. The initial dissociation at $T_L < 26$ °C is specified by k_{eff} given by

$$\frac{1}{k_{eff}(n)} = \frac{1}{m_0 k_0(1)} \exp\left[-\frac{f^*_{tether}(n)\, x_b(1)}{k_BT}\right] + \frac{1}{m_0 k_0(2)} \exp\left[-\frac{f^*_{tether}(n)\, x_b(2)}{k_BT}\right] \quad (22)$$

It strongly depends on the number of bound integrins, m_0 via the $1/m_0$ prefactor as well as the m_0 dependent $f^*_{tether}(n)$ in the exponent. In our numerical estimates, we assume $m_0 \approx 5 \times 10^4$.[37,50,55] The plots of $k_{eff}(n)$ versus n/N demonstrate (Figure 6), as we discussed, a weak effect at $n \approx n_h$ with significant acceleration at $n \approx n_s$. The magnitude of the effect is sensitive to choice of parameters such as m_0 and the precise form of $p_{ventral}(H,z_n)$. However, in the two cases considered, the effective rate is strongly enhanced thus suggesting a robust mechanism.

Our estimates of $f^*_{tether}(n)$ and the corresponding effect on k_{eff} assumed uniform extension of all tethers bearing bound n-RGDs. This assumption is untenable for the ran-RGD case where the n values are randomly distributed. It is nevertheless possible to qualitatively characterize the detachment efficiency of this system by considering the fraction of strongly tensioned integrin−RGD bonds. For simplicity, we consider a brush with h (37 °C) < L_I such that Ψ_{random} (37 °C) ≈ 1 and all RGDs are accessible to cellular integrins. Within our model, integrin−RGD bonds are subject to "efficient" tension at T_L when their tether's polymerization degree n is below n_s, $n \le n_s(T_L) \equiv [h(T_L) - L_I]/Na$. Since the ran-RGDs are randomly placed the fraction of ran-RGDs with a particular $1 \le n \le N$ is $1/N$ and the fraction of ran-RGDs with $n \le n_s$ is (Table 1)

$$\frac{n_s(T_L)}{N} < \frac{h(T_L)}{Na} \sim \left(\frac{a^2}{\Sigma}\right)^{1/3} \quad (23)$$

Importantly, for the typical Σ values we consider, 10 nm^2 ≤ Σ ≤ 50 nm^2, n_s/N varies in the $0.5 \lesssim n_s/N \lesssim 0.5$ range and is typically below 0.3 (Figure 8). In other words, only a minority of the integrin−RGD bonds are subject to efficient tension, thus suggesting slow detachment. We will return to this point in section 4 and Discussion and Conclusions.

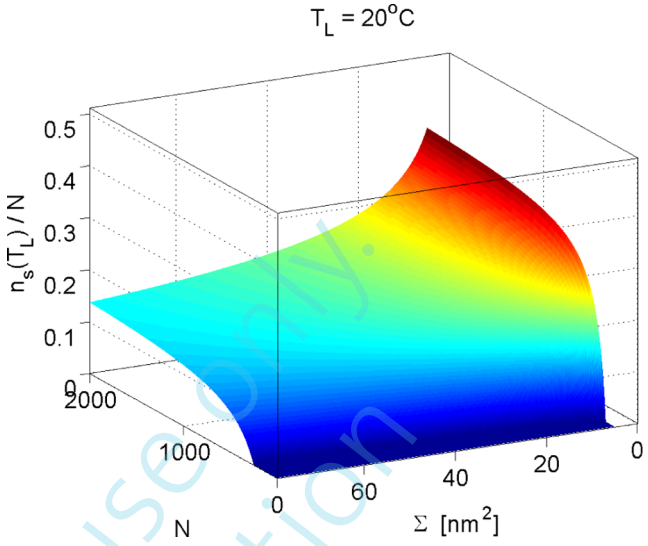

Figure 8. The fraction of ran-RGDs, $n_s(T_L)/N$, experiencing effective tension at T_L = 20 °C, vs Σ and N.

4. DESIGN GUIDELINES OF PNIPAM BRUSH SUBSTRATES

4.1. *n*-RGD. A thermoresponsive cell culture substrate should favor adhesion at 37 °C and enable efficient detachment at $T_L < T_{LCST}$. Within our model, these requirements translate into three design guidelines for n-RGD PNIPAM brushes:

(i) The brush regime should be realized irrespective of T to ensure laterally uniform RGD distribution. Since our analysis is based on the ANB mixing free energy, the brush regime is defined by the overlap threshold of collapsed PNIPAM chains of radius $R_{collapsed} \approx (N/\phi_0)^{1/3}a$ or[37] $R_{collapsed} \approx 0.43N^{1/3}a$ leading to

$$\Sigma < \pi R_{collapsed}^2 \quad (24)$$

This condition is imposed for internal consistency since the ANB free energy predicts chain collapse at $T > T_{LCST}$. It is however important to note experimental results indicating that brushes of low N PNIPAM do not collapse.[56,57]

(ii) To promote adhesion of seeded cells at 37 °C, the n-RGDs should be accessible to cellular integrins, that is, localized at $h(37\ °C) - L_I \le z \le h(37\ °C)$. When $h(37\ °C) \le L_I$, all n-RGDs are accessible and it is thus sufficient to ensure $\sigma_{total} > \sigma_{crit}$. In contrast, $\sigma_{total} > \sigma_{crit}$ is a necessary but insufficient condition when $h(37\ °C) > L_I$ and it is important to consider the effect of brush structure as manifested via $\psi(n)$. The onset of n-RGD accessibility is signaled by n_h such that $\psi(n) = 0$ for all $n \le n_h$. For design purposes, it is however useful to require a finite $\psi(n)$, and we thus utilize $n > n_m(37\ °C)$, eq 8, thus ensuring $\psi(n) \gtrsim 0.6$ at 37 °C. When $L_I < h(37\ °C)$,

dx.doi.org/10.1021/la303443t | Langmuir 2012, 28, 16623−16637

all RGDs are accessible and $n_m(37\ ^\circ\mathrm{C}) = 0$. Note that α_{RGD} should be adjusted to ensure $\sigma_{accessible}(37\ ^\circ\mathrm{C}) > \sigma_{crit}$.

(iii) Cell harvesting at T_L imposes two requirements. One is low n RGD accessibility to ensure that detached cells do not re-adhere. The $\psi(n) = 0$ at T_L condition is satisfied when $n < n_h(T_L)$. The second requirement is efficient detachment of adhering cells cultured at 37 °C. This in turn requires a disjoining force strong enough to significantly accelerate the dissociation rate of integrin−n-RGD bonds. This last requirement can be imposed via $n < n_s$. In turn, $n_s < n_h$ when $\Sigma > \pi p \hat{v} a^2$, and for PNIPAM at 20 °C, with $p = 1$, $a = 0.5$ and $\hat{v} = 1.5$, the condition becomes $\Sigma > 1.2$ nm^2. Accordingly, $n_s < n_h$ in the typical Σ range we consider and the "nonadhesion" condition is redundant.

Combining the three requirements noted above delineates the n/N, Σ regions enabling both adhesion at 37 °C and efficient detachment at T_L (Figure 9). The boundaries vary with N since $n_s(T_L)$ is a function of $N/\Sigma^{1/3}$ while n_m (37 °C) depends Σ/N.

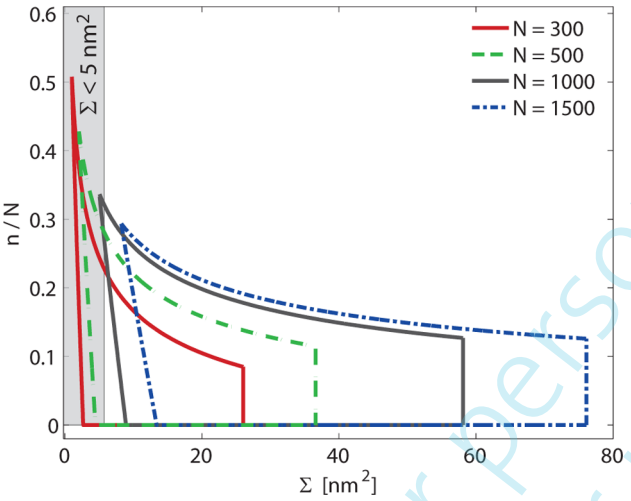

Figure 9. n-RGD brush design diagram for four different N. The upper curved line corresponds to n_s/N at $T_L = 20$ °C (Figure 8), the vertical line delineates the brush boundary (eq 24), while the remaining two lines specify n_m/N at $T = 37$ °C (eq 8) noting that n_m (37 °C) = 0 when $L_I > h(37\ ^\circ\mathrm{C})$. The optimal region is bound within the four lines. The gray $\Sigma < 5$ nm^2 is a rough indication of the practically inaccessible range of high grafting densities.

4.2. ran-RGD. The same performance criteria apply also to ran-RGD brushes. The brush condition is identical. $\psi_{random}(37\ ^\circ\mathrm{C}) \approx 1$ ensuring RGD accessibility and cell adhesion at 37 °C is easily achieved by choosing Σ and N such that $h(37\ ^\circ\mathrm{C}) < L_I$. Nonadhesion at T_L is also straightforward to attain by selecting Σ and N such that $h(T_L) \gg L_I$ and

$$\psi_{random}(T_L) \approx \frac{3}{2}\left(\frac{L_I}{h(T_L)}\right)^2 \sim \left(\frac{L_I}{Na}\right)^2\left(\frac{\Sigma}{a^2}\right)^{2/3} \ll 1 \qquad (25)$$

The inherent difficulty with ran-RGD PNIPAM brushes concerns their tuning for efficient detachment because the fraction of effectively tensioned integrin−RGD bonds is low, $n_s(T_L)/N \sim (a^2/\Sigma)^{1/3}$. In the Σ, N range we explore, the highest $n_s(T_L)/N \approx 0.25$ values are attained for low Σ and high N when $h(37\ ^\circ\mathrm{C}) > L_I$ and $\psi_{random}(37\ ^\circ\mathrm{C}) < 1$ (Figure 10).

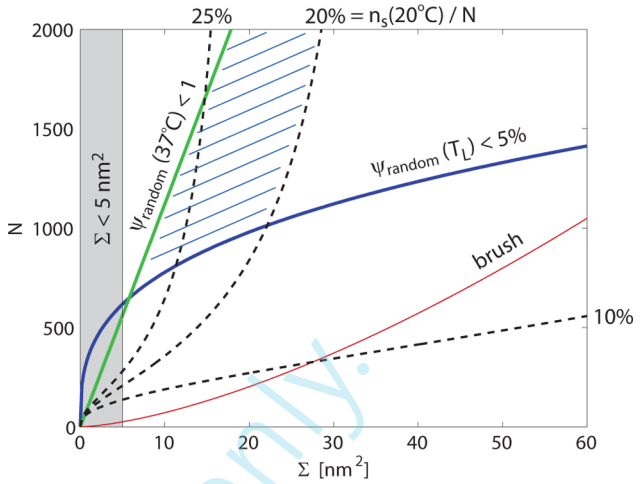

Figure 10. ran-RGD brush design diagram. The broken lines depict the $n_s(T_L)/N = 0.1$, 0.2, 0.25 boundaries. The hatched optimal region is bound by $\psi_{random}(37\ ^\circ\mathrm{C}) = 1$, $\psi_{random}(20\ ^\circ\mathrm{C}) = 0.05$, and $n_s(T_L)/N = 0.2$. Increasing $n_s(T_L)/N$ (cf. Figure 8) diminishes the optimal region, and it is impossible to satisfy all conditions for $n_s(T_L)/N > 0.31$.

5. DISCUSSION AND CONCLUSIONS

Within our model the function of RGD conjugated brushes relates to different facets of brush confinement by the adhering cells. Adhesion of seeded cells is controlled by the RGD fraction accessible to cellular integrins with no brush compression by the ventral membrane. Detachment in the harvesting stage is attributed to disjoining force due to confinement of the swollen brush by cells adhering via integrin−RGD bonds formed when the brush was collapsed, at 37 °C. The performance of RGD brushes can be modeled in some detail for the n-RGD case. The "confinement based" model suggests design guidelines for n/N and Σ of n-RGD brushes promoting cell adhesion at 37 °C and efficient detachment at T_L. While n-RGD are idealization of synthetically conceivable brushes of block copolymers, the underlying mechanism applies to RGD brushes in general and to the ran-RGD case in particular.

The promising performance of nonconjugated PNIPAM brushes suggests the exploration of their RGD conjugated counterparts to achieve thermoresponsive substrates free of xenogenic components. Theoretical considerations of RGD brushes are useful because their design involves multiple parameters thus rendering trial and error exploration inefficient. The study of these systems is also of fundamental interest because their relative simplicity and potential for superior characterization facilitate confrontation with models. In contrast to "serum based" brushes, there is no need to account for the physical adsorption of ECM proteins as well as its dependence on brush structure, T, and time. In distinction to RGD conjugated e-b hydrogels, brushes permit tuning of their structure as well as characterization. Conceptually, n-RGD brushes suggest qualitative tests of the confinement based model. In particular, it predicts that terminal N-RGD will typically promote cell adhesion irrespective of T and produce negligible detachment. Basal 1-RGD (Figure 1) will favor cell adhesion when $h(37\ ^\circ\mathrm{C}) < L_I$ and enable cell detachment when $h(T_L) \gg L_I$.

Our analysis focused on RGD brushes yet to be realized and studied experimentally. In formulating the problem, we drew on

dx.doi.org/10.1021/la303443t | Langmuir 2012, 28, 16623−16637

experimental results concerning e-b hydrogel PNIPAM substrates functionalized by adhesive peptides.[24−26] The efficacy of different adhesive peptides was compared with and without cofunctionalization of insulin. The studies demonstrated that RGD functionalized e-b hydrogels enable cell adhesion/proliferation comparable to the levels attained in serum containing medium. RGD functionalization was made possible by the synthesis of the monomer 2-carboxyisopropylacrylamide (CIPAAm) bearing a pendant COOH group.[58] Free radical polymerization of *N*-isopropylacrylamide (NIPAM) with CIPAAm yields a copolymer with PNIPAM backbone while displaying carboxyl side groups permitting functionalization. Importantly, the copolymers largely retain the phase diagram of PNIPAM. The fraction of COOH bearing monomers was controlled by the CIPAAm/NIPAM ratio in the feed, and the peptides were conjugated to the COOH in a second step using a carbodiimide coupling agent. The fraction of the reacted COOH groups was controlled by the concentration of the free peptide. In the context of our discussion it is helpful to note that nonconjugated PNIPAM brush substrates[9−14] are often produced utilizing surface-initiated atom transfer radical polymerization (SI-ATRP) or surface-initiated reversible-addition fragmentation chain transfer (SI-RAFT) polymerization. The feasibility of using CIPAAm for SI-ATRP or SI-RAFT polymerization is yet to be established. With this caveat in mind, we considered idealizations of brush architectures obtainable via surface-initiated controlled radical polymerization (SI-CRP) reactions[59] allowing to produce grafted-from brushes of diblock and triblock copolymers. The synthesis of diblock brushes with inner RGD conjugated block and poly(methacrylic acid) backbone by using surface-initiated photopolymerization was recently reported.[31] *n*-RGD brushes correspond to such architectures when the RGD conjugated block is short.

Our analysis was motivated by a number of observations concerning e-b PNIPAM hydrogels randomly functionalized by pendant RGD peptides: (i) Cell adhesion at 37 °C increases with x_{RGD} up to a saturation level.[24] (ii) At intermediate x_{RGD}, cell adhesion/proliferation at 37 °C attains the level of PNIPAM brushes in serum containing medium.[24] (iii) The adhesion/proliferation of cells seeded at 20 °C is low and comparable to the level observed on nonfunctionalized e-b hydrogel.[24] (iv) The detachment of cells from RGD hydrogels upon cooling to 20 °C is slower in comparison to the nonfunctionalized e-b hydrogels in serum containing medium.[24,25] (v) For high x_{RGD}, the cell detachment at 20 °C is only partial with up to 70% cell adhering after 24 h incubation. The retardation is observed with both serum free and serum containing culture media.[26] (vi) Estimates of the RGD σ_{total} indicate a large excess in comparison to the σ_{crit} needed to support cell adhesion/proliferation on an impenetrable planar surface, suggesting that many of the RGDs are inaccessible to the cells.[26]

The RGD e-b hydrogels results can be rationalized within our model to the extent that e-b hydrogels can be considered as weakly cross-linked brushes. Adhesion at 37 °C is expected because $h(37\ °C)$ is estimated at 20−30 nm, thus suggesting $0.6 \leq \psi_{random}(37\ °C) \leq 1$ and high RGD accessibility. Nonadhesion at 20 °C is consistent with $\psi_{random}(20\ °C) \ll 1$ and low RGD accessibility. The retarded detachment in comparison to serum based systems is compatible with a low fraction of efficiently tensioned integrin−RGD bonds, $n_s(T_L)/N < 0.5$. Within our description, serum based nonconjugated brushes and hydrogels support cell adhesion due to primary adsorption of ECM proteins at the grafting surface,[37] thus reminiscent of RGD brushes with $1 \leq n \ll N$ and high f^*_{tether}. Importantly, the retarded detachment occurs also in RGD hydrogels in serum containing medium. This suggests that cell adhesion in these systems involves a significant contribution due to high *n* RGDs.

We finally note that the system considered is somewhat reminiscent of brushes undergoing bridging interactions as were considered theoretically in the context of Surface Force Apparatus experiments[60] and of the self-assembly of ABA triblock copolymer mesogels.[61] Our case is however distinctive in two important respects: (i) The bridging interactions involve only a small fraction of the confining surface provided by the cell ventral membrane, that is, $A_{proj}/m_0 \gg \Sigma$. (ii) The bridging sites do not occur at the confining cellular membrane but at the tips of integrin receptors attached to the membrane and extending to a distance of $L_I \approx 20$ nm into the brush.

Overall, our analysis, together with existing experimental results, suggests that controlling the position of the conjugated RGDs is important for the design of RGD conjugated brushes to ensure efficient detachment at T_L as well as adhesion at 37 °C. In practical terms, this suggests exploration of PNIPAM brushes grafted from surfaces prefunctionlized with RGD peptides[62] corresponding to the $n = 1$ case in our discussion. A more demanding direction involves diblock copolymers with a short RGD conjugated block at the vicinity of the grafting surface and a long outward facing nonconjugated block. Such brushes afford the prospect of eliminating the retarded detachment encountered in RGD conjugated e-b hydrogels. Exploring this direction is thus of practical interest for cell sheet engineering. It is also of fundamental value for clarifying the relative roles of mechanisms based on confinement effects and those invoking hydrophobicity/hydrophlicity as characterized by wetting angle measurements.[5,15,63]

APPENDIX A: SCF THEORY

The aim of this Appendix is to recall certain details of the SCF theory and obtain results concerning the position of the *n*th monomer and the corresponding *n*th monomer volume fraction profile $\phi_n(z)$. Within the version of the SCF theory, we utilize[40] the free energy per chain in the brush is

$$\begin{aligned}\frac{F_{chain}}{k_BT} &= \frac{F_{el}}{k_BT} + \frac{F_{int}}{k_BT} \\ &= \frac{3}{2pa^2}\int_0^h dz_N\, g(z_N)\int_0^{z_N} E(z_N, z)\, dz \\ &\quad + \Sigma\int_0^h f_{int}[\phi(z)]\, dz\end{aligned} \tag{26}$$

The first term allows for the elastic free energy of a Gaussian chain while the second reflects the contribution due to monomer−monomer interactions. In the elastic free energy the length $E(z_N,z) = dz/dn$ is proportional to the local tension at z when the chain end is at z_N, $(3k_BT/pa^2)E(z_N,z)$, and n specifies the position of the monomer along the chain. $g(z_N)$ is the probability density function of the altitude of the free ends, z_N. The interaction free energy giving rise to the second term is specified in terms of a free energy density $k_BTf_{int}[\phi(z)]$. In the strong stretching approximation, only chains with $z_N \geq z$ contribute to volume fraction $\phi(z)$ and the three unknown functions specifying the brush are related via

$$\phi(z) = \frac{a^3}{\Sigma}\int_z^h \frac{g(z_N)}{E(z_N, z)}\,\mathrm{d}z_N \tag{27}$$

The brush properties are determined by minimization of F_{chain} subject to two constraints

$$\int_0^{z_N} \frac{\mathrm{d}z}{E(z_N, z)} = N \tag{28}$$

and

$$\frac{\Sigma}{a^3}\int_0^h \phi(z)\,\mathrm{d}z = N \tag{29}$$

The minimization leads to two key equations

$$E(z_N, z) = \frac{\pi}{2N}\sqrt{{z_N}^2 - z^2} \tag{30}$$

and

$$\frac{a^3\partial f_{int}}{\partial\phi} \equiv U(\phi) = \Lambda - (\lambda z)^2 \tag{31}$$

with the characteristic inverse area

$$\lambda^2 \equiv \frac{3\pi^2}{8pa^2N^2} \tag{32}$$

where $U(\phi) = \mu(\phi)/k_BT$ and $\mu(\phi)$ is the parabolic monomer exchange chemical potential. Once Λ is determined via the constraint 29, this last equation allows one to calculate $\phi(z)$ (Table 1).

The position of an n-monomer of a chain whose free end is at z_N is determined by integration of $\mathrm{d}n = 2N\mathrm{d}z/\pi({z_N}^2 - z^2)^{1/2}$ as obtained from eq 30 for $E(z_N,z) = \mathrm{d}z/\mathrm{d}n$. Since $n = 0$ corresponds to $z = 0$, this leads to

$$n(z, z_N) = \frac{2N}{\pi}\arcsin\left(\frac{z}{z_N}\right), \qquad z = z_N\sin\left(\frac{n\pi}{2N}\right) \tag{33}$$

The spatial volume fraction profile of the n-monomer, $\phi_n(z)$, reflects the distribution of free ends $g(z_N)$. Within the SCF theory, n is a continuous parameter and $\phi(z) = \int_0^N \phi_n(z)\mathrm{d}n$ where $\mathrm{d}n = (\partial n/\partial z)(\partial z/\partial z_N)\mathrm{d}z_N = \sin(n\pi/2N)\mathrm{d}z_N/E(z_N,z)$ thus leading to

$$\phi(z) = \sin\left(\frac{n\pi}{2N}\right)\int_z^h \frac{\phi_n(z)}{E(z_N, z)}\,\mathrm{d}z_N \tag{34}$$

Comparison of eq 34 with eq 27 yields $\phi_n(z_N) = g(z_N)a^3/\sin(n\pi/2N)\Sigma$ leading, upon invoking eq 33, to

$$\phi_n(z) = \frac{a^3}{\Sigma}\frac{g\left(z/\sin\left(\frac{n\pi}{2N}\right)\right)}{\sin\left(\frac{n\pi}{2N}\right)} \tag{35}$$

reducing to $\phi_N(z) = g(z)a^3/\Sigma$ for terminal monomers and obeying the normalization condition $\int_0^h \phi_n(z)\mathrm{d}z = a^3/\Sigma$. Since $0 \le z \le h$, the $z/\sin(n\pi/2N)$ dependence of g implies that $\phi_n(z)$ vanishes for $z > h_n$ with

$$h_n \equiv h(T)\sin\left(\frac{n\pi}{2N}\right) \tag{36}$$

thus defining the maximal z populated by the nth monomer.

The mth moment characterizing the $\phi_n(z)$ profile

$$\langle z^m\rangle_n \equiv \frac{\int z^m\phi_n(z)\,\mathrm{d}z}{\int\phi_n(z)\,\mathrm{d}z} = \sin^m\left(\frac{n\pi}{2N}\right)\langle z^m\rangle_N \tag{37}$$

is expressed in terms of the mth moment of g,

$$\langle z^m\rangle_N = \int_0^h z_N^m g(z_N)\,\mathrm{d}z_N \tag{38}$$

and furthermore related to the moments of the $\phi(z)$ profile via

$$\begin{aligned}\langle z^m\rangle &\equiv \frac{\int z^m\phi(z)\,\mathrm{d}z}{\int\phi(z)\,\mathrm{d}z}\\ &= \frac{\Sigma}{Na^3}\int_0^N\int_0^h z^m\phi_n(z)\,\mathrm{d}z\,\mathrm{d}n\\ &= \frac{1}{N}\int_0^N\langle z^m\rangle_n\,\mathrm{d}n\end{aligned} \tag{39}$$

Hence

$$\begin{aligned}\langle z^m\rangle &= \frac{\langle z^m\rangle_N}{N}\int_0^N \sin^m\left(\frac{n\pi}{2N}\right)\mathrm{d}n\\ &= \frac{\Gamma(m/2 + 1/2)}{\sqrt{\pi}\Gamma(m/2 + 1)}\langle z^m\rangle_N\end{aligned} \tag{40}$$

with $\langle z^m\rangle_N$ from eq 38, where Γ is the gamma function with $\Gamma(1) = \Gamma(2) = 1$ and $\Gamma(3/2) = \sqrt{\pi}/2$ thus leading to $\langle z\rangle = 2\langle z\rangle_N/\pi$ and $2\langle z^2\rangle = \langle z^2\rangle_N$.[64] Resubstituting $\langle z\rangle_N$ and $\langle z^2\rangle_N$ into eq 37 leads accordingly to

$$\langle z\rangle_n = \frac{\pi}{2}\langle z\rangle\sin\left(\frac{n\pi}{2N}\right) \tag{41}$$

and

$$\langle z^2\rangle_n = 2\langle z^2\rangle\sin^2\left(\frac{n\pi}{2N}\right) \tag{42}$$

The mean square deviation of the $\phi_n(z)$ profile varies with n

$$\langle z^2\rangle_n - \langle z\rangle_n^2 = \left(2\langle z^2\rangle - \frac{4}{\pi}\langle z\rangle^2\right)\sin^2\left(\frac{n\pi}{2N}\right) \tag{43}$$

and the $\phi_n(z)$ profiles for $n \ll N$ are significantly sharper.

APPENDIX B: THE ANB FREE ENERGY

To describe the behavior of PNIPAM brushes in water, we utilize the empirical ANB[42] f_{int} in the limit of $N \to \infty$ applicable to terminally anchored chains having no translational entropy:

$$a^3 f_{int}(\phi) = (1 - \phi)\ln(1 - \phi) + \chi^{eff}(\phi, T)\,\phi(1 - \phi) \tag{44}$$

with $\chi^{eff}(\phi,T) = \Sigma_k\chi_k(T)\phi^k$ and coefficients

$$\begin{aligned}\chi_0(T) &= -12.947 + 0.044959T/K,\\ \chi_1(T) &= 17.920 - 0.056944T/K,\\ \chi_2(T) &= 14.814 - 0.051419T/K\end{aligned} \tag{45}$$

where T is temperature in Kelvin. The virial expansion of the ANB f_{int} in the form $a^3 f_{int} = v\hat{\phi}^2 + w\hat{\phi}^3 + \ldots$, yields $\hat{v} = 31.4(1 - T/\Theta)$ with $\Theta = 307.81$ K, and thus $\hat{v}$ decreases with increasing T. The third dimensionless virial coefficient is typically negative, $\hat{w} = -2.93(1 - T/W)$ with $W = 532.15$ K, and thus close to -1 at $T = \Theta$. The resulting $\phi(z)$ and $\Pi(z)$ profiles of

dx.doi.org/10.1021/la303443t | Langmuir 2012, 28, 16623−16637

free, unconfined brushes are described in detail in an earlier article.[41] Note that the ANB f_{int} was obtained by fitting the phase boundary of aqueous PNIPAM solutions in the 26 °C $\lesssim T \lesssim$ 35 °C range as obtained from the ANB experimental data later confirmed by Zhou et al.[65] The applicability of this f_{int} outside this T range remains to be established. The ANB f_{int} yields a phase diagram with LCST and UCST with critical points at $\phi_c^{LCST} = 0.413$, $T_{LCST} \approx 26.360$ °C, and $\phi_c^{LCST} \approx 0.661$, $T_{UCST} \approx 15.396$ °C. For $T_L < 26$ °C the U obtained from the ANB theory is well approximated up to an irrelevant constant term by U obtained from $a^3 f_{int} = \hat{v}\phi^2$. When $T > 32$ °C the concentration profile is essentially constant.[41] We find that the volume fraction profile and all other quantities are well represented by the asymptotically poor ($\phi \approx 0.7$) and good ($a^3 f_{int} = \hat{v}\phi^2$) limits at $T = 37$ °C and $T < 26$ °C, respectively (cf. Table 1).

APPENDIX C: ACCESSIBLE FRACTION $\psi(n)$

Substituting $\phi_n(z)$ from eq 35 into the accessible fraction $\psi(n)$ of n-RGDs (eq 2) leads to

$$\psi(n) = \int_{(h-L_1)h/h_n}^{h} g(z_N)\, dz_N \tag{46}$$

For the cases of asymptotic poor and good solvents, where closed forms of $g(z_N)$ are known, it is possible to specify for any particular $\tilde{\psi}$ a $\tilde{n}$ defined via $\psi(\tilde{n}) = \tilde{\psi}$ such that $n > \tilde{n}$ ensures $\psi > \tilde{\psi}$. These $\tilde{n}$ generalize n_m and n_h as discussed in section 2.

$\psi(n)$ in Collapsed Brushes (at 37°C)

In collapsed brushes,[40] $g(z_N) = z_N/h(h^2 - z_N^2)^{1/2}$ leading upon introducing $u = z_N/h$ to

$$\psi(n) = \int_{(h-L_1)/h_n}^{1} u(1-u^2)^{-1/2}\, du = \sqrt{1 - (1 - L_I/h)^2/\sin^2(n\pi/2N)} \tag{47}$$

and

$$\tilde{n} = \frac{2N}{\pi} \arcsin\left(\frac{1 - L_I/h}{\sqrt{1-\tilde{\psi}^2}}\right) \tag{48}$$

Thus $\tilde{n} = h_h$ for $\tilde{\psi} = 0$, while comparing $n_m(37°C)$ as given by eq 8 to $\tilde{n}$ indicates that it corresponds to $\tilde{\psi} \simeq 0.61$.

$\psi(n)$ in Swollen Brushes (at T_L)

In swollen brushes,[40] $g(z_N) = (3u/h)(1-u^2)^{1/2}$ and

$$\psi(n) = \int_{(h-L_1)/h_n}^{1} u(1-u^2)^{1/2}\, du = \sqrt[3]{1 - (1 - L_I/h)^2/\sin^2(n\pi/2N)} \tag{49}$$

leading to

$$\tilde{n} = \frac{2N}{\pi} \arcsin\left(\frac{1 - L_I/h}{\sqrt{1-\tilde{\psi}^{2/3}}}\right) \tag{50}$$

Thus $\tilde{n} = n_h$ for $\tilde{\psi} = 0$ while comparing $n_m(20°C)$ as given by eq 9 to $\tilde{n}$ indicates that it corresponds to $\tilde{\psi} \simeq 0.527$.

APPENDIX D: $z_{n_s}^*$ AND $f_{tether}(z_{n_s}^*)$ AT T_L

At the vicinity of $n \approx n_s$, the tethers are strongly stretched and

$$f_{elastic} \approx \frac{k_B T}{pa} \frac{1}{4(1 - z_n/n_s a)^2} \tag{51}$$

In this regime, $H \lesssim h$ and the leading term in the Taylor expansion of $P(H)$ around $H/h = 1$ is

$$P(H) \approx 9P_0\left(\frac{H}{h} - 1\right)^2 \tag{52}$$

Since $H = z_n + L_I$ and $n_s a = h - L_I$

$$1 - \frac{z_n}{n_s a} = \frac{1 - H/h}{1 - L_I/h} \tag{53}$$

and the mechanical equilibrium condition $m_0 f_{elastic}(z_{n_s}^*) = A_{proj} \times P(z_{n_s}^* + L_I)$ leads to

$$\left(1 - \frac{L_I}{h}\right)^2 = 36\frac{A_{proj}}{m_0}\frac{P_0 a}{k_B T}\left(1 - \frac{H}{h}\right)^4 \tag{54}$$

thus leading to the corresponding entries in eqs 18 and 19.

AUTHOR INFORMATION

Corresponding Author

*E-mail: avraham.halperin@ujf-grenoble.fr (A.H.); mk@mat.ethz.ch (M.K.).

Notes

The authors declare no competing financial interest.

ACKNOWLEDGMENTS

We thank E.B. Zhulina, L. Bureau, and E. Kats for their insightful comments. M.K. acknowledges support by the Swiss National Science Foundation through Grant IZ73Z0-128169.

REFERENCES

(1) da Silva, R. M. P.; Mano, J. F.; Reis, R. L. Smart thermoresponsive coatings and surfaces for tissue engineering: switching cell-material boundaries. *Trends Biotechnol.* **2007**, *25*, 577−583.

(2) Cole, M. A.; Voelcker, N. H.; Thissen, H.; Griesser, H. J. Stimuli-responsive interfaces and systems for the control of protein-surface and cell-surface interactions. *Biomaterials* **2009**, *30*, 1827−1850.

(3) Yang, J.; Yamato, M.; Okano, T. Cell-sheet engineering using intelligent surfaces. *MRS Bull.* **2005**, *30*, 189−193.

(4) Yamato, M.; Akiyama, Y.; Kobayashi, J.; Yang, J.; Kikuchi, A.; Okano, T. Temperature-responsive cell culture surfaces for regenerative medicine with cell sheet engineering. *Prog. Polym. Sci.* **2007**, *32*, 1123−1133.

(5) Nagase, K.; Kobayashi, J.; Okano, T. Temperature-responsive intelligent interfaces for biomolecular separation and cell sheet engineering. *J. R. Soc. Interface.* **2009**, *6*, S293−S309.

(6) Cooperstein, M. A.; Canavan, H. E. Biological cell detachment from poly(*N*-isopropyl acrylamide) and its applications. *Langmuir* **2010**, *26*, 7695−7707.

(7) Yamada, N.; Okano, T.; Sakai, H.; Karikusa, F.; Sawasaki, Y.; Sakurai, Y. Thermoresponsive polymeric surfaces - control of attachment and detachment of clutured cells. *Makromol. Chem. Rapid Commun.* **1990**, *11*, 571−576.

(8) Takezawa, T.; Mori, Y.; Yoshizato, K. Cell-culture on a thermoresponsive polymer surface. *Nat. Biotechnol.* **1990**, *8*, 854−856.

(9) Xu, F. J.; Zhong, S. P.; Yung, L. Y. L.; Kang, E. T.; Neoh, K. G. Surface-active and stimuli-responsive polymer-Si(100) hybrids from surface-initiated atom transfer radical polymerization for control of cell adhesion. *Biomacromolecules* **2004**, *5*, 2392−2403.

(10) Mizutani, A.; Kikuchi, A.; Yamato, M.; Kanazawa, H.; Okano, T. Preparation of thermoresponsive polymer brush surfaces and their interaction with cells. *Biomaterials* **2008**, *29*, 2073−2081.

(11) Li, L.; Zhu, Y.; Li, B.; Gao, C. Fabrication of Thermoresponsive Polymer Gradients for Study of Cell Adhesion and Detachment. *Langmuir* **2008**, *24*, 13632−13639.
(12) Takahashi, H.; Nakayama, M.; Yamato, M.; Okano, T. Controlled chain length and graft density of thermoresponsive polymer Brushes for Optimizing Cell Sheet Harvest. *Biomacromolecules* **2010**, *11*, 1991−1999.
(13) Nagase, K.; Watanabe, M.; Kikuchi, A.; Yamato, M.; Okano, T. Thermo-responsive polymer brushes as intelligent biointerfaces: Preparation via ATRP and characterization. *Macromol. Biosci.* **2011**, *11*, 400−409.
(14) Xue, C.; Choi, B.-C.; Braun, P. V.; Kong, Q.; Leckband, D. E. Protein adsorption modes determine reversible cell attachment on poly(N-isopropylacrylamide) brushes. *Adv. Funct. Mater.* **2012**, *22*, 2394−2401.
(15) Nakayama, M.; Yamada, N.; Kumashiro, Y.; Kanazawa, H.; Yamato, M.; Okano, T. Thermoresponsive Poly(*N*-isopropylacrylamide) Based Block Copolymer Coating for Optimizing Cell Sheet Fabrication. *Macromol. Biosci.* **2012**, *12*, 751−760.
(16) Canavan, H. E.; Cheng, X. H.; Graham, D. J.; Ratner, B. D.; Castner, D. G. Cell sheet detachment affects the extracellular matrix: A surface science study comparing thermal liftoff, enzymatic, and mechanical methods. *J. Biomed. Mater. Res.* **2005**, *75A*, 1−13.
(17) Cheng, X. H.; Canavan, H. E.; Stein, M. J.; HullJ, J. R.; Kweskin, S. J.; Wagner, M. S.; Somorjai, G. A.; Castner, D. G.; Ratner, B. D. Surface chemical and mechanical properties of plasma-polymerized *N*-isopropylacrylamide. *Langmuir* **2005**, *21*, 7833−7841.
(18) Canavan, H. E.; Cheng, X. H.; Graham, D. J.; Ratner, B. D.; Castner, D. G. Comparison of native extracellular matrix with adsorbed protein films using secondary ion mass spectrometry. *Langmuir* **2007**, *23*, 50−56.
(19) Reed, J. A.; Love, S. A.; Lucero, A. E.; Haynes, C. L.; Canavan, H. E. Effect of polymer deposition method on thermoresponsive polymer films and resulting cellular behavior. *Langmuir* **2012**, *28*, 2281−2287.
(20) Okajima, S.; Sakai, Y.; Yamaguchi, T. Development of a Regenerable Cell Culture System That Senses and Releases Dead Cells. *Langmuir* **2005**, *21*, 4043−4049.
(21) Schmidt, S.; Zeiser, M.; Hellweg, T.; Duschl, C.; Fery, A.; Möhwald, H. Adhesion and mechanical properties of PNIPAM microgel films and their potential use as switchable cell culture substrates. *Adv. Funct. Mater.* **2010**, *20*, 3235−3243.
(22) Mannello, F.; Tonti, G. A. Concise Review: No Breakthroughs for Human Mesenchymal and Embryonic Stem Cell Culture: Conditioned Medium, Feeder Layer, or Feeder-Free; Medium with Fetal Calf Serum, Human Serum, or Enriched Plasma; Serum-Free, Serum Replacement Nonconditioned Medium, or Ad Hoc Formula? All That Glitters Is Not Gold! *Stem Cells* **2007**, *25*, 1603−1609.
(23) Wilson, C. J.; Clegg, R. E.; Leavesley, D. I.; Pearcy, M. J. Mediation of biomaterial-cell interactions by adsorbed proteins: A review. *Tissue Eng.* **2005**, *11*, 1−18.
(24) Ebara, M.; Yamato, M.; Aoyagi, T.; Kikuchi, A.; Sakai, K.; Okano, T. Immobilization of cell-adhesive peptides to temperature-responsive surfaces facilitates both serum-free cell adhesion and noninvasive cell harvest. *Tissue Eng.* **2004**, *10*, 1125−1135.
(25) Ebara, M.; Yamato, M.; Aoyagi, T.; Kikuchi, A.; Sakai, K.; Okano, T. Temperature-responsive cell culture surfaces enable "on-off" affinity control between cell integrins and RGDS ligands. *Biomacromolecules* **2004**, *5*, 505−510.
(26) Hatakeyama, H.; Kikuchi, A.; Yamato, M.; Okano, T. Bio-functionalized thermoresponsive interfaces facilitating cell adhesion and proliferation. *Biomaterials* **2006**, *27*, 5069−5078.
(27) Hatakeyama, H.; Kikuchia, A.; Yamatoa, M.; Okanoa, T. Patterned biofunctional designs of thermoresponsive surfaces for spatiotemporally controlled cell adhesion, growth, and thermally induced detachment. *Biomaterials* **2007**, *28*, 3632−3643.
(28) Milner, S. T. Polymer brushes. *Science* **1991**, *251*, 905−914.
(29) Lai, P.-Y.; Zhulina, E. Monte Carlo test of the self-consistent field theory of a polymer brush. *J. Phys. II* **1992**, *2*, 547−560.
(30) Tugulu, S.; Silacci, P.; Stergiopulos, N.; Klok, H. A. RGD - functionalized polymer brushes as substrates for the integrin specific adhesion of human umbilical vein endothelial cells. *Biomaterials* **2007**, *28*, 2536−2546.
(31) Navarro, M.; Benetti, E. M.; Zapotoczny, S.; Planell, J. A.; Vansco, G. J. Buried, covalently attached RGD peptide motifs in poly(methacrylic acid) brush layers: The effect of brush structure on cell adhesion. *Langmuir* **2008**, *24*, 10996−11002.
(32) Wei, Y.; Ji, Y.; Xiao, L. L.; Lin, Q. K.; Ji, J. Different complex surfaces of polyethyleneglycol (PEG) and REDV ligand to enhance the endothelial cells selectivity over smooth muscle cells. *Colloids Surf., B* **2011**, *84*, 369−378.
(33) Shin, H.; Jo, S.; Mikos, A. G. Biomimetic materials for tissue engineering. *Biomaterials* **2003**, *24*, 4353−4364.
(34) Xiong, J.-P.; Stehle, T.; Diefenbach, B.; Zhang, R. G.; Dunker, R.; Scott, D. L.; Joachimiak, A.; Goodman, S. L.; Arnaout, M. A. Crystal structure of the extracellular segment of integrin $\alpha_V\beta_3$. *Science* **2001**, *294*, 339−345.
(35) Xiong, J.-P.; Stehle, T.; Zhang, R. G.; Joachimiak, A.; Frech, M.; Goodman, S. L.; Arnaout, M. A. Crystal structure of the extracellular segment of integrin $\alpha_V\beta_3$ in complex with an Arg-Gly-Asp ligand. *Science* **2002**, *296*, 151−155.
(36) Halperin, A. Polymer brushes that resist adsorption of model proteins: Design parameters. *Langmuir* **1999**, *15*, 2525−2533.
(37) Halperin, A.; Kröger, M. Theoretical considerations on mechanisms of harvesting cells cultured on thermoresponsive polymer brushes. *Biomaterials* **2012**, *33*, 4975−4987.
(38) Bell, G. I. Models for specific adhesion of cells to cells. *Science* **1978**, *200*, 618−627.
(39) Evans, E.; Williams, P. In *Physics of bio-molecules and cells*; Jülicher, F., Ormos, P., David, F., Flyvbjerg, H., Eds.; Springer: Berlin, 2002; pp 145−204.
(40) Zhulina, E. B.; Borisov, O. V.; Priamitsyn, V. A. Theory of the steric stabilization of colloid dispersions by grafted polymers. *J. Colloid Interface Sci.* **1990**, *137*, 495−511.
(41) Halperin, A.; Kröger, M. Collapse of thermoresponsive brushes and the tuning of protein adsorption. *Macromolecules* **2011**, *44*, 6986−7005.
(42) Afroze, F.; Nies, E.; Berghmans, H. Phase transitions in the system poly(N-isopropylacrylamide)/water and swelling behavior of the corresponding networks. *J. Mol. Struct.* **2000**, *554*, 55−68.
(43) Toomey, R.; Tirrell, M. Functional polymer brushes in aqueous media from self-assembled and surface-initiated polymers. *Annu. Rev. Phys. Chem.* **2008**, *59*, 493−517.
(44) Yim, H.; Kent, M. S.; Satija, S.; Mendez, S.; Balamurugan, S. S.; Balamurugan, S.; Lopez, G. E. Evidence for vertical phase separation in densely grafted, high-molecular-weight poly(N-isopropylacrylamide) brushes in water. *Phys. Rev. E* **2005**, *72*, 051801.
(45) Yim, H.; Kent, M. S.; Mendez, S.; Lopez, G. P.; Satija, S.; Seo, Y. Effects of grafting density and molecular weight on the temperature-dependent conformational change of poly(N-isopropylacrylamide) grafted chains in water. *Macromolecules* **2006**, *39*, 3420−3426.
(46) Koga, T.; Tanaka, F.; Motokawa, R.; Koizumi, S.; Winnik, F. M. Theoretical modeling of associated structures in aqueous solutions of hydrophobically modified telechelic PNIPAM based on a neutron scattering study. *Macromolecules* **2008**, *41*, 9413−9422.
(47) Iwanaga, Y.; Braun, D.; Fromherz, P. No correlation of focal contacts and close adhesion by comparing GFP-vinculin and fluorescence interference of dil. *Eur. Biophys. J.* **2001**, *30*, 17−26.
(48) Li, F.; Redick, S. D.; Erickson, H. P.; Moy, V. T. Force measurements of the $\alpha_5\beta_1$ integrin-fibronectin interaction. *Biophys. J.* **2003**, *84*, 1252−1262.
(49) Massia, S. P.; Hubbell, J. A. An RGD spacing of 440 nm is sufficient for integrin alpha V beta 3-mediated fibroblast spreading and 140 nm for focal contact and stress fiber formation. *J. Cell Biol.* **1991**, *114*, 1089−1100.
(50) Moore, S. W.; Roca-Cusachs, P.; Sheetz, M. P. Stretchy proteins on stretchy substrates: The important elements of integrin-mediated rigidity sensing. *Dev. Cell* **2010**, *19*, 194−206.

(51) Halperin, A.; Zhulina, E. B. Atomic force microscopy of polymer brushes: colloidal versus sharp tips. *Langmuir* **2010**, *26*, 8933−8940.
(52) Marko, J. F.; Siggia, E. D. Stretching DNA. *Macromolecules* **1995**, *28*, 8759−8770.
(53) Yamamoto, S.; Tsujii, Y.; Fukuda, T. Atomic Force Microscopic Study of Stretching a Single Polymer Chain in a Polymer Brush. *Macromolecules* **2000**, *33*, 5995−5998.
(54) Evans, E.; Ritchie, K. Strength of a weak bond connecting flexible polymer chains. *Biophys. J.* **1999**, *76*, 2439−2447.
(55) Arnold, M.; Cavalcanti-Adam, E. A.; Glass, R.; Eck, W.; Kantlehner, M.; Kessler, H.; Spatz, J. P. Activation of integrin function by nanopatterned adhesive interfaces. *ChemPhysChem* **2004**, *5*, 383−388.
(56) Zhu, X.; Yan, C.; Winnik, F. M.; Leckband, D. E. End-grafted low-molecular-weight PNIPAM does not collapse above the LCST. *Langmuir* **2007**, *23*, 162−169.
(57) Plunkett, K. N.; Zhu, X.; Moore, J. S.; Leckband, D. E. PNIPAM chain collapse depends on the molecular weight and grafting density. *Langmuir* **2006**, *22*, 4259−4266.
(58) Aoyagi, T.; Ebara, M.; Sakai, K.; Sakurai, Y.; Okano, T. Novel bifunctional polymer with reactivity and temperature sensitivity. *J. Biomater. Sci. Polym. Ed.* **2000**, *11*, 101−110.
(59) Barbey, R.; Lavanant, L.; Paripovic, D.; Schüwer, N.; Sugnaux, C.; Tugulu, S.; Klok, H.-A. Polymer Brushes via Surface-Initiated Controlled Radical Polymerization: Synthesis, Characterization, Properties, and Applications. *Chem. Rev.* **2009**, *109*, 5437−5527.
(60) Johner, A.; Joanny, F. Adsorption of polymeric brushes: Bridging. *J. Chem. Phys.* **1992**, *96*, 6257−6273.
(61) Zhulina, E. B.; Halperin, A. Lamellar mesogels and mesophases: a self-consistent-field theory. *Macromolecules* **1992**, *25*, 5730−5741.
(62) Bureau, L. Private communication.
(63) Okano, T.; Yamada, N.; Okuhara, M.; Sakai, H.; Sakurai, Y. Mechanism of cell detachment from temperature-modulated, hydrophilic-hydrophobic polymer surfaces. *Biomaterials* **1995**, *16*, 297−303.
(64) Skvortsov, A. M.; Pavlushkov, I. V.; Gorbunov, A. A.; Zhulina, Y. B.; Borisov, O. V.; Pryamitsyn, V. A. Structure of densely grafted polymeric monolayers. *Polym. Sci. USSR* **1988**, *30*, 1706−1715.
(65) Zhou, X.; Li, J.; Wu, C.; Zheng, B. Constructing the Phase Diagram of an Aqueous Solution of Poly(*N*-isopropyl acrylamide) by Controlled Microevaporation in a Nanoliter Microchamber. *Macromol. Rapid Commun.* **2008**, *29*, 1363.